

FINAL REPORT

AFOSR Grant # F49620-96-1-0286

**PHASE STABILITY AND MICROSTRUCTURAL DESIGN IN
HIGH TEMPERATURE (Mo,Nb)-Si-B ALLOYS**

Professor John H. Perepezko, Principal Investigator

Department of Materials Science and Engineering

University of Wisconsin – Madison

1509 University Avenue, Madison WI 53706

19991101 046

REPORT DOCUMENTATION PAGE

AFRL-SR-BL-TR-99-

0254

maintaining
ons for
Office of

Public reporting burden for this collection of information is estimated to average 1 hour per response, including the time for reviewing the data needed, and completing and reviewing this collection of information. Send comments regarding this burden estimate reducing this burden to Washington Headquarters Services, Directorate for Information Operations and Reports, 1215 Jefferson Management and Budget, Paperwork Reduction Project (0704-0188), Washington, DC 20503

1. AGENCY USE ONLY (Leave blank)		2. REPORT DATE October 15, 1999	3. REPORT TYPE AND DATES COVERED Final Report, 1 July 1996 - 30 June 1999	
4. TITLE AND SUBTITLE Phase Stability and Microstructure Design in High Temperature (Mo,Nb)-Si-B Alloys			5. FUNDING NUMBERS F49620-96-1-0286	
6. AUTHOR(S) Prof. J. H. Perepezko, Principal Investigator				
7. PERFORMING ORGANIZATION NAME(S) AND ADDRESS(ES) University of Wisconsin - Madison Dept. of Materials Science and Engineering, 1509 University Ave., Madison, WI 53706			8. PERFORMING ORGANIZATION REPORT NUMBER	
9. SPONSORING / MONITORING AGENCY NAME(S) AND ADDRESS(ES) AFOSR / NA 801 North Randolph St. Arlington, VA 22203 - 1977 Attn. Dr. S. Wu			10. SPONSORING / MONITORING AGENCY REPORT NUMBER	
11. SUPPLEMENTARY NOTES				
12a. DISTRIBUTION / AVAILABILITY STATEMENT DISTRIBUTION STATEMENT A Approved for Public Release Distribution Unlimited			12b. DISTRIBUTION CODE	
13. ABSTRACT (Maximum 200 Words) The challenges of a high-temperature ($T > 1400^{\circ}\text{C}$) environment impose severe constraints on materials selection in terms of melting temperature, oxidation resistance and structural functionality. In order to satisfy these criteria, refractory metal silicides that can develop adherent SiO_2 oxidation layers emerge as the most attractive candidates. However, multiphase microstructure designs must be applied to address the toughening and strengthening issues that must be resolved for the use of refractory metal silicides. In the current work, a stable two-phase equilibrium between Mo and a Mo_5SiB_2 intermetallic (T_2) phase has been established. While this stability is an attractive attribute, it is also a challenge in developing processing strategies that will allow for the manipulation of microstructure in order to achieve designs that will offer enhanced performance at high temperature. New microstructure control based solidification processing (including rapid solidification) has been demonstrated. An in-situ precipitation reaction to yield Mo dispersions within the Mo_5SiB_2 intermetallic phase has been discovered and found to be effective in enhancing strength and toughness.				
14. SUBJECT TERMS Refractory Metal Alloys, Structural Materials, Mo Alloys, Oxidation Resistance, High Temperature, Multiphase, Microstructure, Intermetallics			15. NUMBER OF PAGES 60	
			16. PRICE CODE	
17. SECURITY CLASSIFICATION OF REPORT	18. SECURITY CLASSIFICATION OF THIS PAGE	19. SECURITY CLASSIFICATION OF ABSTRACT	20. LIMITATION OF ABSTRACT	

TABLE OF CONTENTS

Abstract	2
1) Introduction	3
2) Approach	5
3) Research Highlights	
3.1 Liquidus Projection on the Mo-rich portion of Mo-B-Si Ternary System	7
3.2 Solidification pathways of (Mo(ss) + T ₂) two-phase alloys	8
3.3 Development of Mo(ss) + T ₂ Two-Phase Microstructure	10
3.4 Development of Single-phase T ₂	12
3.5 Mo(ss) precipitation in the T ₂ phase	14
3.6 Precipitation Enhanced Toughening	18
3.7 Assessment of the diffusion behavior involving the T ₂ phase formation	19
3.8 Phase Stability of the Mo-rich Mo-Si-B system at 1600°C	22
3.9 Thermodynamic Evaluation of the Phase Equilibria in the Mo-rich Mo-Si-B system	23
3.10 Phase Equilibria in the Nb-rich side of the Nb-Si-B System at 1600°C	27
3.11 Solidification Reaction Sequence in the Nb(ss) + T ₂ two-phase field of the Nb-rich Nb-Si-B alloys	28
3.12 Phase Investigation on (Mo,Nb) + T ₂ two-phase field	29
4) Summary of Research Highlights	31
5) Publication List	33
6) References	35
7) Appendix	39
8) Tables	42
9) Figures	44

Phase Stability and Microstructure Design in High Temperature

(Mo,Nb)-Si-B Alloys

Abstract

The challenges of a high-temperature ($T > 1400^\circ\text{C}$) environment impose severe constraints on materials selection in terms of melting temperature, oxidation resistance and structural functionality. In order to satisfy these criteria, refractory metal silicides that can develop adherent SiO_2 oxidation layers emerge as the most attractive candidates. However, multiphase microstructure designs must be applied to address the toughening and strengthening issues that must be resolved for the use of refractory metal silicides. In the current work, a stable two-phase equilibrium between Mo and a Mo_5SiB_2 intermetallic (T_2) phase has been established. While this stability is an attractive attribute, it is also a challenge in developing processing strategies that will allow for the manipulation of microstructure in order to achieve designs that will offer enhanced performance at high temperature. New microstructure control based solidification processing (including rapid solidification) has been demonstrated. An in-situ precipitation reaction to yield Mo dispersions within the Mo_5SiB_2 intermetallic phase has been discovered and found to be effective in enhancing strength and toughness.

1 - Introduction

In an elevated temperature environment, the essential requirements for a structural material aside from the obvious one of high melting point include high temperature strength, stiffness and oxidation resistance at low density, but adequate room temperature mechanical properties and cost effectiveness are also critical factors. Intermetallic alloys, especially the titanium aluminide alloys, have attracted a great deal of interest for these applications. However, for titanium aluminides the main applications are limited to temperatures below 1000°C. The most significant payoffs in terms of advanced aerospace applications and engine uses require temperatures well above that for the titanium aluminides and approaching the range of 1400°C - 1500°C [88Via, 86Hep].

High temperature service requires a thermal stability of the constituent phases which can be considered from several points of view. First and foremost is survivability which clearly requires an inherently high melting temperature. In addition, a limited interaction with the service environment and compatibility with oxidation resistant coatings or with reinforcement phases in composites are often basic requirements for survivability of a component at high temperature. Moreover, application induced microstructural modification due to thermal cycling and the combined effects of temperature excursions under varying stress states are important to consider for a useful component. The underlying basis for alloy synthesis, processing and the assessment of thermal stability is established by the relevant phase equilibria in all systems.

It is apparent that all of the above mentioned requirements may not be satisfied by a single phase alloy system, but instead may be achieved by using a multiphase design

with a tailored microstructure. The performance of multiphase alloys is governed by the characteristics of their internal interfaces which in turn are greatly influenced by the interaction among the existing phases in the alloys. Clearly the success of superalloys is based upon a carefully balanced multiphase design. In order to achieve an effective combination of mechanical, chemical and morphological stability a knowledge of the relevant phase diagrams is essential. On the basis of these diagrams it is possible to select combinations of phases which may possess the desired properties. Kinetic data are also required to understand and to control the possible interphase/interface reactions and the evolution of microstructure during phase transformations. With this approach a systematic and knowledge-based assessment of advanced materials may be pursued which is essential for successful development [92Dim].

Based upon several general, but critical, criteria involving central materials characteristics and performance metrics for high temperature use, a candidate refractory metal system based upon ternary Mo-Si-B alloys has been identified as attractive to examine in a systematic fundamental study of phase stability. In this system as well as the companion Nb-Si-B system a ternary intermetallic $(\text{Mo,Nb})_5\text{SiB}_2$, T_2 phase has been reported to coexist with a refractory metal solution phase. During the current program the initial report has been tested and confirmed in a systematic investigation of phase stability and microstructure control based upon the following objectives:

Examination of Phase Stability in the Mo-Si-B System

- a) evaluation of the phase equilibria for the Mo-rich section of the Mo-B-Si system at 1600°C and 1200°C.

- b) determination of the solidification pathways in the Mo-rich section of the Mo-B-Si system with emphasis on the Mo(ss) + T₂ two-phase field region.
- c) examination of the high-temperature diffusion characteristics involved in the Mo(ss) + T₂ two-phase alloys.
- d) investigation of phase stability in the companion Nb-Si-B system.

Investigation of Microstructural Development in Mo(ss)+T₂ Alloys

- a) evaluation of microstructural modification of the two-phase alloys utilizing the rapid solidification processing (RSP).
- b) evaluation of solid-state phase transformation involved in the two-phase field region.
- c) analysis on the structure and crystallography of the (Mo,Nb)(ss)/T₂ interface via High-Resolution Transmission Electron Microscopy (HRTEM).

As a background for the proposed renewal program which is intended to examine several key outstanding issues in phase stability, microstructure control and processing in detail, a summary of the research highlights of the current work provides an important perspective. At the same time, it is also useful to reiterate the materials selection criteria.

From this background it is evident that the promise of the initial expectations and findings has been realized in large measure. Indeed, the research program in the current study has also served to define a number of important outstanding issues, challenges and opportunities in the development of (Mo,Nb)-Si-B alloys for high temperature applications. In fact, some of the outstanding issues relate to the remarkable phase and microstructural stability observed at high temperature. While this stability is an attractive attribute, it is also a challenge in developing processing strategies that will allow for the manipulation of microstructure in order to achieve designs that will offer enhanced

performance at high temperature. The experience in the current work allows for the identification of a detailed examination of solidification microstructure development and control, the control over an in-situ precipitation process that has been discovered in the current work, the kinetic analysis of diffusion behavior, the thermodynamic analysis of phase stability and the application of microstructure control to the synthesis of new microstructure morphologies and designs for high temperature service as key objectives to pursue during the renewal effort in fundamental studies on (Mo,Nb)-Si-B alloys.

The approach that has been established in the current work based upon complimentary experimental approaches including: DTA, long term annealing, diffusion couples, EPMA measurements, rapidly solidified samples and electron microscopy will be applied in the proposed renewal study. Throughout the intended effort a close collaboration will be maintained with UTRC and P&W in related efforts on mechanical properties and upscale sample sizes. The outcome of the three-year effort has provided an assessment of microstructural modification potential and critical guidance for successful materials processing in this promising high temperature materials system.

2) Approach

All alloy compositions are prepared by non-consumable arc melting of pure Mo, Nb, Si and B in a titanium gettered argon atmosphere. The ingots are subjected to multiple meltings in order to insure complete dissolution of the components. To expedite the approach to equilibrium at relatively low annealing temperature, some of the alloys are rapidly solidified via splat quenching. The arc-cast samples and the splats are coated with

Y_2O_3 , wrapped in Ta foil, placed in an Al_2O_3 crucible and heat treated in an Al_2O_3 tube furnace at 1200°C and 1600°C for 150 hours. Both splat quenching and drop-tube processing are being employed to evaluate the extent of microstructural tailoring that can be attained via RSP. Annealing treatments at 1600°C for varying time are conducted to evaluate solid-state reactions and the resulting structures are characterized by using SEM, XRD and TEM. The structure and the crystallographic relationships between $(\text{Mo,Nb})_{\text{ss}}$ and T_2 have been elucidated using HRTEM and Fourier-filtered images. In an effort to map out phase reaction sequences, selected diffusion couples have been designated to identify component diffusivities in the T_2 phase. The diffusion couples are assembled in Ta foil wrapping and annealed at 1600°C for varying times and subsequently furnace cooled. The diffusion couples are sectioned perpendicular to the initial interface using a diamond impregnated low speed saw. In order to avoid carbon and/or silicon contamination, the section diffusion couple was polished with only 12 and 1 μm Al_2O_3 powder. In order to determine the phase compositions in equilibrated alloys and to assess the diffusion path that evolves during interdiffusion, EPMA/WDA analysis is being conducted on certain samples.

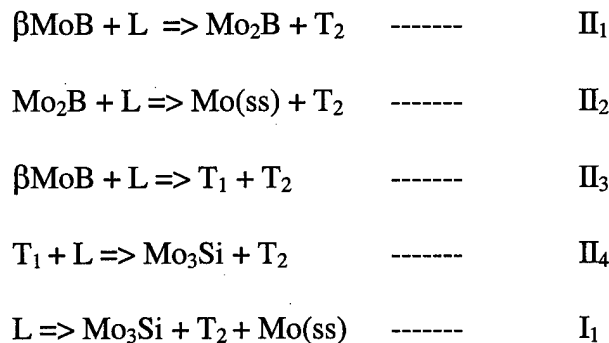
3. Research Highlights

During the current work a detailed experimental investigation of the fundamentals of phase stability and microstructure control has been pursued into the focus areas listed in the program objectives. A summary of this work is important not only in establishing the promising potential of $(\text{Mo,Nb})\text{-Si-B}$ alloys, but also in identifying the challenges and

new opportunities that have been defined in the current work. Indeed, the outstanding challenges and opportunities are the basis for the proposed continuing effort. A major part of this work is published (see publication list) so that only the central points are summarized.

3.1 Liquidus projection on the Mo-rich portion of Mo-B-Si Ternary System

The liquidus projection in the Mo-rich portion of the Mo-Si-B ternary system phases have been examined based on the microstructures of arc-cast alloys. The liquidus projection in the Mo-rich portion involve six primary solidification reactions; five reactions originated from the Mo-Si and Mo-B binary sections (Mo, Mo₂B, βMoB, Mo₃Si and Mo₅Si₃) and one from the ternary-based T₂ phase (figure 1). The liquidus surface in general descends from the higher melting Mo-B binary side to the lower melting Mo-Si binary side. The several liquidus surfaces such those of T₂ and Mo₃Si phases appear to be quite shallow. The solidification path of the T₂ phase compositions is always proceeded by the MoB primary and subsequently the peritectic reaction of βMoB + L => T₂. Four Class II reactions (quasi-peritectic reactions) and one Class I reaction (an invariant ternary eutectic reaction) have been identified as follows:



With regards to the solidification processing of the Mo(ss) + T₂ two-phase alloys, several solidification paths involving additional phases such as Mo₂B, MoB and Mo₃Si phases have been observed. A more detailed examination on the solidification pathways involved in the two-phase field is described in the following section.

3.2 Solidification pathways of as-cast alloys in the (Mo(ss) + T₂) two-phase field

The solidification pathways of alloys in the two-phase field of Mo(ss) and T₂ phase have been characterized by the severe segregation which involves the formation of additional phases such as Mo₂B, MoB, Mo₃Si and Mo₅Si₃ during conventional casting (arc-melting) [97Per, 97Nun]. Based on our assessment on the Mo-rich portion of Mo-B-Si liquidus surface and the estimated Mo-T₂ quasi-binary section from analysis of the solidification structures (see Figure 2), four types of solidification pathways involving different primary phases have been identified within this region depending on the composition as follows:

1. For Mo alloys with $0 < B < 14$ at. % and $0 < Si < 7$ at. %:
Mo(ss) non-faceted dendritic primary > Mo(ss) + Mo₂B eutectics > Mo(ss) + T₂ eutectics > Mo₃Si + T₂ co-precipitation.
2. For Mo alloys with $14 < B < 19$ at. % and $7 < Si < 8.5$ at. % :
Mo₂B faceted columnar primary > Moss + Mo₂B co-precipitation > Moss + T₂ eutectics > Mo₃Si + T₂ co-precipitation.
3. For Mo alloys with $19 < B < 22.5$ at. % and $8.5 < Si < 11.25$ at. % :
T₂ faceted columnar primary > Moss + T₂ eutectics > Mo₃Si + T₂ co-precipitation

4. For Mo alloys with $19 < B < 22.5$ at. % and $8.5 < Si < 11.25$ at. % :

MoB dendritic primary $> T_2$ (via a peritectic reaction of $MoB + L > T_2$) $> Mo_3Si$
 + T_2 co-precipitation

Although there is a transition in primary phase selection with changing composition across the $Mo(ss) + T_2$ two phase field, the final solidification reaction in the sequence always involves the co-precipitation of $Mo_3Si + T_2$ as a eutectic with the Mo_3Si phase as the matrix. The formation of Mo_3Si as the matrix in the eutectic can be understood by the fact that the initial solidification involves the formation of boride phases. Following the initial solidification the liquid composition has shifted toward Si-rich levels so the subsequent solidification follows the $Mo(ss) + T_2$ eutectic through until reaching the completion of reaction in the $Mo_3Si + T_2$ region. Hence, the limiting composition of the remaining microstructure allows for a relatively large volume fraction of Mo_3Si as a non-equilibrium segregation induced constituent.

The presence of Mo_3Si as a matrix in the final eutectic solidification reaction, in addition to the formation of Mo_2B and MoB during the earlier stages of solidification, hinders the equilibration process during subsequent solid state annealing. The segregation induced binary borides and silicides exhibit sluggish dissolution kinetics. In fact, experience has demonstrated that annealing at $1600^\circ C$ for 150 hours is barely sufficient to dissolve the Mo_3Si and Mo_2B phases [97Per]. Even after this extended annealing treatment, the microstructures of the resulting alloys are not uniform as shown in figure 15. Moreover, it is also evident that extended annealing at $1200^\circ C$ yields almost no change in the as-cast microstructure. Since the issue of solidification segregation is a major point in assessing the phase stability in the Mo-Si-B system some means of

reducing the extent of segregation and the formation of non-equilibrium constituents is essential. As described in the next section a strategy based upon the application of rapid solidification methods has been demonstrated to be most effective in achieving this objective and allowing for a reliable assessment of the phase stability.

3.3 Development of Mo(ss) + T₂ Two-Phase Microstructure

The production of a two-phase (Mo(ss) + T₂) microstructure directly from the arc-melted alloys has been shown to be severely restricted as indicated in previous sections. Furthermore, an extensive annealing process is required to dissolve the additional phases that are formed in the arc-cast alloys due to the low diffusion rates even at relatively high temperatures. This experience presents a great challenge in high temperature materials. Although high temperature characteristics such as microstructural stability and low diffusion rates (of the order of 10^{-15} to 10^{-16} m²/s) [99Kim] are desirable in these alloys, the attainment of the two-phase microstructures necessitates an extensive subsequent annealing processing at very high temperatures. Moreover, the phase equilibria at relatively low temperatures is difficult to ascertain due to the low mobility of species involved in the system. Hence, an alternative material processing is required to facilitate the attainment of two-phase microstructures at low temperatures. In particular, a materials processing method that yields a much shorter diffusion path is certainly beneficial.

Rapid Solidification Processing (RSP) such as splat quenching (SQ) can be utilized to produce alloys with more refined and homogeneous microstructures. More importantly, RSP has been frequently used to obtain high melt undercooling and rapid

interface velocities such that solidification segregation can be successfully suppressed. As indicated in the previous section, the solidification pathways of the arc-melted $\text{Mo}_{70}\text{B}_{20}\text{Si}_{10}$ alloy are initiated by the T_2 primary and followed by the formation of $\text{Mo}(\text{ss}) + \text{T}_2$ monovariant eutectic and $\text{Mo}_3\text{Si} + \text{T}_2$ co-precipitation (see Figure 3). In contrast, the resulting SQ alloys with a similar composition exhibited a refined two-phase microstructure as shown in Figure 4 a and confirmed by XRD measurements (Figure 4 b). Two types of microstructures corresponding to the level of undercooling attained can be discerned. Near the edge of the splat foil, a coupled-growth of the $\text{Mo} + \text{T}_2$ was detected. No T_2 dendritic structure can be observed. This can be associated with the most undercooled regime wherein the formation of T_2 primary dendritic phase can be suppressed and Mo and T_2 phase can grow cooperatively. Upon the completion of the coupled-growth regime, the T_2 phase forms either a cellular structure with the Mo phase or a dendritic structure that was subsequently followed by the formation of the $\text{Mo} + \text{T}_2$ eutectic. The x-ray traces of the splat-quenched alloy indicated the presence of Mo and T_2 peaks only. Thus, the segregation problem associated with the formation of Mo_3Si phase by conventional processing means can be circumvented by rapid solidification. The annealing treatment at 1200°C for 150 hours resulted in a uniform duplex microstructure consisting of Mo dispersions in a T_2 matrix (see Figure 5). This is in stark contrast to the arc-melted alloys annealed with a similar procedure which showed the solidification microstructure with Mo_3Si being maintained after annealing at 1200°C . The feasibility of producing a $\text{Mo}(\text{SS})+\text{T}_2$ two-phase microstructure directly from the melt via an RSP technique is clearly demonstrated by this experience. Furthermore, the application of RSP

to all of the compositions under study has used to develop the isotherm phase diagram sections at 1600°C.

3.4 Development of Single-phase T₂

It is desirable to examine the possibility of producing the T₂-phase directly from the melt. As noted in the Mo-T₂ plethral section (see Figure 2), the T₂ phase melts incongruently so that MoB would solidify first in as-cast alloys with a T₂-stoichiometric composition (Mo_{62.5}B₂₅Si_{12.5}). The solidification path then proceeds with T₂ phase formation through a peritectic reaction of MoB + L ⇒ T₂. Mo₃Si and Mo₅Si₃ phases would then also form as the last parts to solidify. Hence, the production of T₂ phase via conventional casting would be very challenging due to severe solidification segregation involving phases such as MoB and Mo₅Si₃ which exhibit sluggish dissolution. In fact, arc-melted alloys with this composition still maintained the four phases in the microstructures even upon annealing at 1600°C for 150 hours as shown in Figure 6. Thus, similar to the Mo(ss) + T₂ two-phase alloys, the single-phase T₂ formed via conventional casting requires an extensive annealing procedure at very high temperature i.e. in excess of 150 hours at 1600°C.

For these conditions, RSP can be again very useful in suppressing the solidification segregation through the development of high melt undercooling and rapid interface velocities. Splat-quenched alloys with a T₂ stoichiometric composition, in contrast to the as-cast alloys, exhibited only a single T₂ phase. This was confirmed by the XRD measurements indicating only the T₂ phase in splat samples (see Figure 7). Thus,

T_2 phase can be successfully produced directly from the melt provided that a sufficient level of undercooling can be attained to suppress the primary solidification of MoB and secondary phase formation of Mo_3Si and Mo_5Si_3 .

3.5 Mo(ss) Precipitation in the T_2 phase

As noted in the figure 8, the as-cast microstructure for $Mo_{70}B_{20}Si_{10}$ shows three phases: primary faceted Mo_5SiB_2 (T_2) phase, Mo(ss) and Mo_3Si . The Mo(ss) phase represents about 0.45 volume fraction of the (Mo(ss) + T_2) eutectic region and about 0.2 volume fraction of the overall microstructure. In the as-cast condition TEM examination did not detect Mo(ss) precipitates in the T_2 primary phase. In samples annealed at 1600°C for 25 hours, there was a clear indication for the formation of Mo(ss) precipitates in the T_2 primary phase (see Figure 8a). A prominent feature was the plate-like shape of the Mo(ss) precipitates. The precipitates varied in length from 1.0 to 3.0 μm . The thickness of the precipitates was less than 0.2 μm . A tendency to form a high precipitate density near the edge of the T_2 primary phase was clearly evident (see region A in Figure 8b). In addition, an apparent precipitate-free-zone (PFZ) is also noted in the T_2 phase immediately adjacent to the (Mo(ss) + T_2) eutectic structure (region B in Fig. 8b).

Alloys annealed at 1600°C for 150 hours (see Figure 8c) developed a microstructure with a high density of Mo(ss) precipitates near the edge and a relatively sparse precipitate density at the center of the T_2 phase (region A in Figure 8c). The length of the precipitates varied from 3.0 to 7.0 μm . Unlike the lengthening process, the thickening process of the precipitates was relatively slow.

A TEM observation showed that the Mo(ss) precipitates develop facets (see Figure 8c). A number of different crystallographic orientations for the Mo precipitates within the T_2 matrix were indicated by electron diffraction analysis. However, most of the plate-like precipitates showed the following relations (see Figure 8e and 8f):

$$\text{Mo(ss)} \{111\} \parallel T_2 (001); \text{Mo(ss)} [01\bar{1}] \parallel T_2 [110], \quad (1a)$$

$$\text{Mo(ss)} \{111\} \parallel T_2 (001); \text{Mo(ss)} [01\bar{1}] \parallel T_2 [1\bar{1}0]. \quad (1b)$$

For the Mo(ss) precipitates with the above orientation relations the Mo(ss)/ T_2 interface was identified to be approximately parallel to a Mo(ss){211} plane (for the long Mo(ss)/ T_2 interface of the plate like Mo(ss) precipitates, see Figure 3a) and to a Mo{110} plane (for the short interface). In the T_2 matrix the interfaces are parallel to the T_2 {110} planes.

The relative sluggishness of the microstructure change of the $\text{Mo}_{70}\text{B}_{20}\text{Si}_{10}$ alloy at high temperatures is readily apparent. This is due to the low diffusion rates in this system which contribute to a remarkable microstructural stability. However, the same sluggish diffusion also plays a key role in the slow dissolution rate of Mo_3Si phase and the attainment of equilibrium. As previously shown [97Per, 97Nun], the Mo_3Si phase formation can be suppressed by the use of rapid solidification processing (RSP). The formation of Mo(ss) precipitates during heat treatment in the solid state demonstrates that a significant supersaturation can be retained within the T_2 matrix and that the T_2 phase can not be considered as a line compound. The precipitation reaction is an important finding since it allows for the further development of toughening strategies for this system [94Cha].

The observations on the development of Mo(ss) precipitates within the T_2 phase are consistent with the sketch of the Mo(ss) + T_2 quasi-binary phase diagram in Figure 2 and the stability of the T_2 phase over a composition range. Upon solidification, the initial formation of primary T_2 phase occurs with little supersaturation of Mo. During continued freezing of the primary T_2 , the composition tracks the solidus to yield increasing levels of Mo. The cooling conditions during arc-melting of small ingots are sufficiently rapid to suppress the development of the Mo_2B phase so that the segregation of Mo in the primary T_2 phase continues to the extent given by the monovariant eutectic. The sluggish solid state diffusion in this system allows for the segregation profile in T_2 to be retained after final solidification. With this pathway the greatest Mo segregation and hence the largest supersaturation level in the T_2 primary would develop at the end of the primary solidification as the path changes to co-precipitation of the (Mo(ss) + T_2) eutectic. In fact, the microstructure does show clearly (see Figure 8b) that the highest precipitate density does develop near the edge of the T_2 primary phase. At the same time an apparent precipitate free zone develops within the T_2 primary adjacent to the (Mo(ss) + T_2) eutectic structure. The extent of this zone (i.e. about 1.0–1.5 μm) can be understood if the Mo supersaturation due to segregation in the T_2 phase is diminished by diffusional relaxation (in the vicinity of the zone). This would imply a diffusivity of the order of 10^{-18} m^2/s which is reasonable for a Mo-base alloy at 1600°C [79Mei].

A TEM/SAED analysis on the annealed samples demonstrates that most of the Mo(ss) precipitates have specific orientations within the T_2 matrix (see eq. (1)) and a $T_2/\text{Mo(ss)}$ interface approximately parallel to a $\text{Mo(ss)}\{211\}$ plane and to a $T_2\{110\}$ plane for the long interface of the plate like precipitates (see Figure 9a). These

orientations allow for the formation of a semi-coherent Mo(ss)/T₂ interface with a lattice mismatch between the opposite Mo(ss) (110) planes (0.2250 nm) and T₂ (220) planes (0.2131 nm) of 4.43 % (the lattice misfit is defined as $(a_{\text{Mo}} - 0.5a_{\text{T}_2})/0.5a_{\text{T}_2}$ where a_{Mo} and a_{T_2} are the lattice parameters of Mo(ss) and T₂ phases respectively in annealed Mo₇₀B₂₀Si₁₀ alloys). In the Fourier-filtered image in Figure 9b the Mo(ss)(110) and T₂(220) reflections were used to show details of the dislocation structure in the Mo(ss)/T₂ interface. The filtered image shows a semi-coherent Mo(ss)/T₂ interface interrupted by a periodic arrangement of misfit dislocations. The Mo(ss)/T₂ lattice mismatch is accommodated by T₂ (220) extra lattice planes that end at the Mo/T₂ interface and show a spacing of about 4.8 nm in average (approximately 23 T₂ (220) planes equal to about a 4.4% mismatch compensation). Thus, the interfacial dislocation structure yields more than 94% accommodation of the Mo(ss)/T₂ lattice mismatch. It should be mentioned that the semi-coherent character of the planar Mo(ss)/T₂ interface remains even after a prolonged annealing treatment (i.e. at a temperature of 1600°C for 150 hours).

The lengthening kinetics appears to be more extensive than the thickening of the precipitates based on microstructures of alloys annealed at 1600°C at 25 and 150 hours. The slow thickening rate can be attributed to the presence of an interfacial barrier at the planar Mo(ss)/T₂ semi-coherent interface that apparently can be maintained even after a relatively long annealing time. The relative immobility of the partially coherent Mo(ss)/T₂ interface also promotes the development of a plate morphology [78Aar]. The remarkable stability of the precipitate morphology and precipitate/matrix interface structure are attractive features for high temperature service applications.

The formation of dispersed ductile precipitates with a relatively high aspect ratio should provide an important contribution to the damage tolerance of (intermetallic + ductile) two phase alloys such as Mo(ss) + T₂ [94Cha, 91Dev]. The mechanism of microstructural evolution of the plate-like precipitate is currently being examined. An understanding on the mechanism will enable the development of effective strategies for the control of the morphology and the density of the plates by annealing procedure and alloying.

3.6 Precipitation Enhanced Toughening in Mo(ss) + T₂ Alloys

A preliminary indentation test with a load of 1 kg on Mo₇₀B₂₀Si₁₀ alloys indicated the benefits from Mo(ss) precipitates in the T₂ matrix. Crack bridging in the T₂ matrix by Mo(ss) precipitates was observed (see Figure 10). This mechanism should provide important contribution to the overall toughness of the microstructures. Indeed, the optimal condition with respect to the toughening mechanism can only be obtained by the presence of dense Mo(ss) precipitates in the T₂ matrix. Thus, very short annealing treatment at higher temperatures would be required to promote a high nucleation density of Mo(ss) precipitates.

The role of the Mo phase distribution in a T₂ matrix to influence further crack propagation resistance can be demonstrated by a Vickers indentation test (load of 300 g) on the SQ foil (see Figure 12). The crack propagation apparent in the arc-cast ingot was effectively inhibited due to the homogeneous distribution of Mo phase in the T₂ matrix in the SQ foil. This experience further emphasized the importance of high density of Mo

phase precipitates uniformly dispersed in the T_2 phase. In this case again, RSP has been essential to facilitate the development of a homogeneous Mo phase distribution conducive to microstructural toughening.

3.7 Assessment on the diffusion behavior involving the T_2 phase formation

In the current work, a diffusion study has been initiated to examine the formation of the T_2 phase based upon reaction (b) between Mo_2B and Mo_5Si_3 . Figure 11 shows the back-scattered (BS) image of the cross section of the diffusion couple taken by the secondary electron microscopy (SEM) between Mo_5Si_3 and Mo_2B after annealing treatment at 1600C for 400 hours. The EPMA analysis proves the Mo_2B phase on the far-left side and Mo_5Si_3 on the far-right side. Diffusion reaction between Mo_2B and Mo_5Si_3 produces two product phases in a diffusion couple annealed at 1600°C for 100 and 200 hours respectively. In 400 hour annealed diffusion couple, one single phase T_2 appears in between Mo_2B and Mo_5Si_3 . According to the EPMA analysis, the two product phases in a diffusion couple annealed for 100 hours or 200 hours turn out to be T_2 and Mo_3Si . The product phase next to the Mo_2B phase is T_2 . The Mo_3Si phase appears next to the Mo_5Si_3 phase. The EPMA analysis also shows that the product phase in a diffusion couple annealed for 400 hours is T_2 . The T_2 phase shows flat interface with Mo_2B even though it grows into columnar structure (Figure 11). The T_2 phase, however, does not have flat interface with Mo_5Si_3 . In addition, the columnar grains close to the Mo_5Si_3 are bigger than those to the Mo_2B phase. Moreover, cracks in Mo_5Si_3 are stopped or diverted at the

interface between Mo_3Si and Mo_5Si_3 and the interface between T_2 and this indicates that T_2 and Mo_3Si have a toughness level sufficient to reduce crack propagation.

The Mo_3Si phase is found on the Mo_5Si_3 side in 100 and 200 hours annealed diffusion couples, but is not uniformly produced along the Mo_5Si_3 phase (Figure 12). On the contrary, the Mo_3Si phase was not found in a diffusion couple annealed for 400 hours. The Mo_3Si phase is formed on the Mo_5Si_3 phase side, and the T_2 phase is produced on the Mo_2B phase side due to Si atomic flow. However, the disappearance of Mo_3Si after long term annealing seems to indicate that B atoms diffuse faster than Si atoms. This is supported by results from a diffusion couple of $\text{Mo}_2\text{B}/\text{Mo}_5\text{Si}_3$ annealed at 1700°C for 182 hours. Figure 25 shows BSE images of the Mo_3Si phase existing (a)&(b) along the T_2 phase and (c)&(d) partially between T_2 and Mo_5Si_3 in the $\text{Mo}_2\text{B}/\text{Mo}_5\text{Si}_3$ diffusion couple annealed at 1700°C for 182 hours. This indicates that directional movement of faster B atoms transform the partial region of Mo_3Si into T_2 (Figure 12 (c) & (d)).

A key consequence of the changing phase sequence with annealing time is that the initial diffusion path is not the steady state path, but reflects transient conditions. The path that appears to represent steady state is given in Figure 13. The associated composition profile is shown in Figure 14 along with the analytical representation of the composition profile that can be used to evaluate the diffusion coefficients based on analysis given in the appendix as:

$$\begin{aligned}
 D_{\text{SiSi}}^{\text{Mo}} &= 1.61 \times 10^{-15} \text{ m}^2/\text{sec} & D_{\text{SiB}}^{\text{Mo}} &= 5.14 \times 10^{-16} \text{ m}^2/\text{sec} \\
 D_{\text{BSi}}^{\text{Mo}} &= -1.77 \times 10^{-15} \text{ m}^2/\text{sec} & D_{\text{BB}}^{\text{Mo}} &= -5.32 \times 10^{-16} \text{ m}^2/\text{sec}
 \end{aligned}$$

or

$$D_{SiSi}^B = 1.10 \times 10^{-15} \text{ m}^2/\text{sec} \quad D_{SiMo}^B = -5.14 \times 10^{-16} \text{ m}^2/\text{sec}$$

$$D_{MoSi}^B = 1.42 \times 10^{-16} \text{ m}^2/\text{sec} \quad D_{MoMo}^B = -1.80 \times 10^{-17} \text{ m}^2/\text{sec}$$

The self diffusion coefficient of Mo in a pure Mo is $1.49 \times 10^{-17} \text{ m}^2/\text{sec}$ [83Smi]. When atoms in a homogeneous system such as a pure element or an alloy are placed in a constant chemical potential field, the energy barriers for atoms to move to adjacent sites are identical. The only way to move to adjacent sites is by thermal jumping. If atoms move via a vacancy mechanism, they may thermally jump into adjacent vacant sites because there are local concentration differences due to vacancies. As a consequence, the component interdiffusion coefficients tend to be larger than the self diffusion coefficient of Mo.

The overall growth kinetics for the T_2 phase is presented in Figure 15 and demonstrates diffusion control. The solid line in Figure 15 was obtained using the interdiffusion coefficients of the T_2 phase and the theoretical solution for the solute concentration derived by Fujita *et al* [56Fuj]. The estimated growth rate constant for T_2 is $9 \times 10^{-16} \text{ m}^2/\text{sec}$ at 1600°C . According to Bartlett *et al* [64Bar], the growth rate constant of Mo_3Si is approximately $3.75 \times 10^{-14} \text{ m}^2/\text{sec}$ at 1600°C . The growth rate of T_2 is about two orders of magnitude lower than that of Mo_3Si . Moreover, as indicated in Figure 16 the growth behavior of the T_2 layer is influenced by the neighboring phases which change with time during annealing as the diffusion path approaches steady state. Thus, the

extrapolation of short time growth behavior to long times is questionable. This effect is also likely to impact the analysis and interpretation of oxidation behavior.

3.8 Phase Stability of the Mo-rich Mo-Si-B system at 1600°C

Based upon the results presented in the previous sections concerning the long term annealing of as-cast samples, the examination of rapidly solidified samples, x-ray diffraction determination of phase identity and lattice parameter trends and the EPMA examination of phase compositions in the isothermal section for the Mo-Si-B system at 1600°C has been constructed as shown in Figure 16. Since the boundary lines are plotted on the basis of composition data of homogeneous phases obtained using EPMA, the boundaries are drawn as a broken line. Moreover, the present study concentrates on the Mo-MoB-Mo₅Si₃ region excluding the two-phase equilibrium region of MoB-Mo₅Si₃. Accordingly the ternary isothermal section in Figure 16 does not contain a complete boundary of MoB-Mo₅Si₃ two-phase equilibrium region. This gives incomplete compositional boundaries of both the B-rich side of MoB and the Si-rich side of Mo₅Si₃. The compositional region of Mo₂B extends from ~33 at%B to ~38 at%B and its solubility of Si reaches to about 1 at%Si. The composition boundary of the Mo-rich side of MoB reaches ~51 at%B and the solubility of Si reaches up to about 2 at%Si. The Mo(ss) phase does have negligible solubility of B but appreciable solubility of Si up to about 3 at%Si. The Mo₃Si phase has compositional homogeneity region from ~22 at%Si to ~26 at%Si and negligible solubility of B. The compositional boundary of the Mo-rich side of Mo₅Si₃

extends to ~35at%Si. In addition, the T₂ phase has solubility of Si from ~9 at%Si up to ~13 at%Si as well as solubility of B from ~24 at%B up to ~32 at%B.

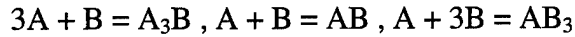
3.9 Thermodynamic Evaluation of the Phase Equilibria in the Mo-rich Mo-Si-B system

In order to provide a basis for the reliable analysis of the measured phase stability and to provide guidance in the further analysis and interpretation of the character of the defect structure in the T₂ phase an evaluation of the thermodynamic properties is necessary. Unfortunately, reliable thermodynamic data for the T₂ phase are not available. However, some data on the phases that coexist in equilibrium with the T₂ phase (Figure 16) is available and may be used to establish reasonable bounds on the free energy of formation of the T₂ phase. To serve as background on this approach, the evaluation method is illustrated for a binary alloy and then extended to the ternary Mo-Si-B system. The final result does demonstrate that the main features of the phase stability observed at 1600°C can be reproduced by the thermodynamic calculation. At the present stage there are also clear limitations on the calculation method since it treats phases as line compounds. However, the approach does illustrate the potential for a full analysis once measurements become available. In fact, some of the proposed work has been developed in order to supply the measurements needed for a more complete thermodynamic evaluation.

In Mo-Si, Mo-B and Si-B binary phase diagrams [92Asm], the stable phases at 1600°C are Mo, Si, B, Mo₂B, MoB, MoB₂, Mo₂B₅, MoB₄, SiB_n, Mo₃Si, Mo₅Si₃ and MoSi₂. In the Mo-Si-B ternary equilibrium shown in Figure 15, a unique ternary phase

Mo_5SiB_2 (T_2) exists as a stable phase at 1600°C . Although the Mo-B binary phase diagram contains MoB_2 and MoB_4 as a stable phase at 1600°C , the ternary isothermal section of the Mo-Si-B system drawn by Nowotny does not include those phases.

To begin with, a method estimating the unknown free energy of formation of a phase in a binary A-B system is illustrated. Let us suppose that there are 5 stable phases - A, A_3B , AB, AB_3 and B (Figure 17) with negligible solubility of nonstoichiometry. The system contains the equilibria



and the free energies of formation of A_3B and AB_3 phases with respect to the standard states of pure A and pure B are known except AB. $g_{f,i}$ denotes the free energy of formation of i . The tangential line between A_3B and AB_3 geometrically illustrates that the free energy of formation of the stable AB phase ($g_{f,AB}$) can vary in ranges between $g_{f,AB}^1$ and $-\infty$. The tangential lines between A and A_3B , and AB_3 and B are intercepted at the composition of AB ($X_B = 0.5$). The tangential intercepts geometrically divide the stability region of AB into three areas. Each area shows different stability as follows.

- When $-\infty < g_{f,AB} < g_{f,AB}^3$, the AB phase produces tangential relations with A and B respectively. The binary A-B system contains stable A, AB and B phases, and metastable A_3B and AB_3 phases.
- When $g_{f,AB}^3 < g_{f,AB} < g_{f,AB}^2$, the AB phase produces tangential relations with A and AB_3 . The binary A-B system contains stable A, AB, AB_3 and B phases, and a metastable A_3B phase.

- When $g_{f,AB}^2 < g_{f,AB} < g_{f,AB}^1$, the AB phase produces tangential relations with A_3B and AB_3 . The binary A-B system finally contains stable A, A_3B , AB, AB_3 and B phases.

In order for phases A, A_3B , AB, AB_3 and B to be stable, the free energy of formation of AB has a value in between $g_{f,AB}^1$ and $g_{f,AB}^2$. Usually, the mean value $(\frac{g_{f,AB}^1 + g_{f,AB}^2}{2})$ is used as the estimate for $g_{f,AB}$.

Using the thermodynamic data (Table 1) and the following thermodynamic relations

$$S_T = S_{298} + \int_{298}^T \frac{C_p}{T} dT$$

$$\Delta H_T = \Delta H_{298} + \int_{298}^T C_p dT$$

the free energy of formation of each phase at 1600°C is evaluated (Table 2). The free energy of formation of Mo_2B_5 is estimated from the free energy diagram of the Mo-B binary system. In order for Mo_2B , MoB and Mo_2B_5 to be stable at 1600°C, the rational value of the free energy of formation of Mo_2B_5 should be in between -93.09 and -130.55 KJ/g-atom. The mean value, -111.82 KJ/g-atom, is selected as the free energy of formation of Mo_2B_5 at 1600°C. Each phase in the Mo-Si-B system with nonstoichiometric composition range has stoichiometric composition. On the basis of the phase stability shown in Figure 17, the free energy of formation of the T_2 phase is estimated as -130.9 ± 0.6 KJ/g-atom (or -1047.30 ± 5.29 KJ/mole). A linear regression on the free energies of formation of the T_2 phase at other temperatures (Table 3) gives

$$\Delta G_f = -100.34 - 0.505T \text{ (KJ/mole) for the } T_2 \text{ phase}$$

The free energy planes of phases in the Mo-rich Mo-Si-B system including the T_2 phase can be established using the sub-lattice model, developed by Hillert and Staffanson [70Hil] based on Temkin's model for ionic solutions [45Tem] and extended by Sundman and Agren [81Sun]. Ansara *et al.* [97Ans] and Huang [98Hua] shows that the sub-lattice model is very adequate to describe the thermodynamic properties of the ordered phases in the Ni-Al system which is characterized by five intermetallic compounds with different structures.

In addition, the fact that the activities of Mo, Si and B respectively have constant values in a three-phase equilibrium region indicates that the activities in that region are easily estimated using an equilibrium reaction among phases. A consideration of estimated activity values of a component establishes its stability diagram illustrating the chemical potential (or activity) changes with respect to composition. Since the chemical potential changes during reaction affects the diffusion pathway and path sequence, knowledge of chemical potential variation of a component as a function of composition is significant. Generally, constant chemical potential of each component (e.g. A, B and C) in a three-phase equilibrium (e.g. α - β - γ equilibrium) gives

$$G^\alpha = X_A^\alpha \mu_A + X_B^\alpha \mu_B + X_C^\alpha \mu_C \quad \text{at three-phase equilibrium composition}$$

of α phase

$$G^\beta = X_A^\beta \mu_A + X_B^\beta \mu_B + X_C^\beta \mu_C \quad \text{at three-phase equilibrium composition}$$

of β phase

$$G^\gamma = X_A^\gamma \mu_A + X_B^\gamma \mu_B + X_C^\gamma \mu_C \quad \text{at three-phase equilibrium composition}$$

of γ phase

Consideration of α , β and γ phases as a line compound indicates that G^j is the free energy of formation of j phase ($j = \alpha, \beta$ or γ) and X_i^j is the mole fraction of component i ($i = A, B$ or C) at stoichiometry of j phase. Solving linear equations, then, yields the values of constant chemical potentials in the α - β - γ three-phase equilibrium region. Based upon this analysis method and the schematic isothermal section of the Mo-Si-B system at 1600°C (Figure 18), the stability diagrams of Mo, Si and B can be obtained.

3.10 Phase Equilibria in the Nb-rich side of the Nb-Si-B System at 1600°C

The evaluation of the phase relations in the Nb-rich side of the Nb-Si-B system at 1600°C focused on confirming the existence of the Nb(ss) + T_2 two-phase field. The results are based on the analysis of the following alloys Nb-6.5Si-3.5B (#1), Nb-15Si-5B (#2), Nb-10Si-10B (#3), Nb-15Si-15B (#4), Nb-20Si-10B (#5), Nb-25Si-5B (#6), Nb-12Si-18B (#7), Nb-27Si-3B (#8), Nb-12.5Si-25B (#9), Nb-25Si-12.5B (#10), Nb-31Si-6.5B (#11), Nb-34.5Si-3.5B (#12), Nb-18Si-21B (#13), Nb-17.5Si-B (#15), Nb-21Si-16.5B (#18), Nb-17.5Si-20B (#19), Nb-5Si-25B (#20), Nb-19Si-1B (#21), and Nb-7Si-13B (#22) (all compositions in atomic %). The Nb-rich portion of the Nb-Si-B 1600°C isothermal section according to Nowotny [60Now] is shown in Figure 19. The compositions of our alloys are indicated on the same figure. The phase identification was determined using XRD and SEM metallography. The T_2 phase XRD peaks were matched using the Mo_5SiB_2 XRD data. Alloy #1 consisted of a two-phase microstructure of

primary Nb(ss) and a eutectic of Nb(ss) and T_2 . Alloys #2, #3, #4, #5, and #6 consisted of a two-phase microstructure of primary T_2 and a eutectic of Nb(ss) and T_2 . Alloys #8, #10, #11, #12 and #15 consisted of a three phase microstructure of primary $\beta\text{Nb}_5\text{Si}_3$ (T_1 phase), T_2 from a peritectic reaction of $L + \beta\text{Nb}_5\text{Si}_3$, and a eutectic of Nb(ss) and T_2 . Alloys #7, #9, #13, #18, #19, and #20 consisted of a three phase microstructure of primary NbB, T_2 from a peritectic reaction of $L + \text{NbB}$, and a eutectic of Nb(ss) and T_2 in the as-cast condition.

It was found that most of the two-phase field could be reached upon solidification. Heat treatment of the alloys at 1600°C for 150 hours produced slight coarsening of the eutectic microstructure. In the alloys near the T_2 single-phase field (alloys #9, #10, #11, #12, #18, and #19), the primary phase (either NbB or Nb_5Si_3) dissolved along with some of the eutectic, increasing the amount of T_2 phase present. The results therefore confirmed the large range of two-phase field in the Nb-Si-B system as previously assessed [60Now]. The Nb_3B_2 phase was not detected in any of the alloys through XRD, which is in contrary to the original diagram.

3.11 Solidification Reaction Sequence in the Nb(ss) + T_2 two-phase field

The solidification sequence has been examined in Nb-rich Nb-Si-B alloys produced by non-consumable electrode arc melting. Through SEM/BSE and XRD microstructural characterization, four types of primary solidification can be identified: Nb(ss), T_2 , NbB, and Nb_5Si_3 .

Alloys that are near the T_2 composition form either NbB or Nb_5Si_3 directly from the liquid. In the Nb-Si-B system, Nb_5Si_3 (2520°C) has a higher melting point than NbB (~2320°C). In contrast, MoB (~2600°C) has a higher melting point than Mo_5Si_3 (2180°C) in the Mo-Si-B system. Since the near- T_2 compositions always solidify with either primary NbB or Nb_5Si_3 , it would stand to reason that the melting point of the T_2 phase is less than the melting point of NbB or Nb_5Si_3 .

The most interesting feature of the solidification is that an as-cast microstructure consisting of Nb(ss) and T_2 can be formed. Either primary Nb(ss) or T_2 can be formed depending on which side of the eutectic the composition is located. This allows for easy adjustment of the microstructure in order to achieve the desired properties. If toughness was important, then a microstructure containing primary Nb(ss) could easily be produced in the as-cast condition. If oxidation resistance in a stronger material is desired, a microstructure containing primary T_2 could also be easily produced in the as-cast condition.

3.12 Phase Investigation on the (Mo,Nb) + T_2 two-phase field

Phase investigation on the two-phase field involving (Mo,Nb)_{ss} and T_2 phases in the Mo-Nb-B-Si system has been initiated. The starting material used was Mo-20B-10Si (at. %) which contains about 80 % of T_2 phase and 20% of Mo at 1600°C. Varying amounts of Nb were added to replace the Mo content in the alloys with compositions of (70-x)Mo-xNb-20B-10Si. The annealed alloys at 1600°C indicated the presence of mainly the two phases with some solidification remnants of (Mo,Nb)₃Si. The XRD

results indicated the continuous increase in crystal sizes of the T_2 phase with increasing Nb content (see Figure 20). Hence, based on these initial results, it appears that the T_2 phase from Mo-B-Si ternary system and the Nb-B-Si ternary system forms a continuous solid solution and that two phase field of (Mo,Nb) and T_2 are indeed stable at 1600°C. It is important also to point out the preferential partitioning of Nb solute to the T_2 phase. As the Nb content is increased, the corresponding increase in lattice parameters from the T_2 phase are higher considerably than those from the (Mo,Nb) phase. This finding may be provide an additional degree of microstructural control in the (Mo,Nb) + T_2 two-phase alloys.

It is interesting to note here also that in the case of Mo-Nb-Si system, the solubility extension of the binary T_2 phase from Nb-Si side (Nb_5Si_3) was severely limited due to the stabilization of the T_1 phase of Nb_5Si_3 . In fact, the reported quasi-binary section of $Nb_5Si_3 - Mo_5Si_3$ [65Sav] indicated that T_1 should be stable even at much lower temperatures than 1650°C (the transition temperature of $T_1 \leftrightarrow T_2$ in Nb-Si side). Therefore, boron apparently exhibits a profound effect in destabilizing the T_1 phase in the quaternary system and stabilizing the T_2 phase and the two-phase field.

With regards to the metalloid contents in the T_2 phase, it appears that the variations in B and Si solubility may be attributed to the strict geometrical requirement attached to the stabilization of the T_2 structure. This can be supported by the fact that the c/a ratio of the T_2 phase quite constant in all of these alloys (see Fig. 21) in spite of the continuous increase in the lattice parameters as shown in Fig. 20.

The increase in lattice parameters due to substitution of Mo by a larger atom Nb may yield a corresponding increase in the volume of interstitial sites within the T_2 phase.

This may facilitate a larger versatility in the metalloid solubility in the T_2 phase. In this context, the Nb addition can be accompanied by a larger solubility of the larger sized Si atoms in the T_2 phase as noted in Nb-B-Si system wherein the T_2 phase is indeed much more Si rich than that in Mo-B-Si system. This point is being carefully evaluated to explore the possibility of applying this rule to alloying for (Mo(ss) + T_2) alloys.

4 - Summary of Research Highlights

1. The challenges of a high temperature environment limit materials selection choices to refractory metals, intermetallics and ceramics. When the additional constraints of oxidation resistance and functionality as a structural component are considered, refractory metal silicides emerge as perhaps the most attractive option. To address the deficiencies in mechanical performance of silicides including low temperature brittleness and high temperature creep resistance, multiphase microstructural designs appear to offer viable approaches in order to take advantage of ductile phase toughening and dispersion strengthening. These approaches must be implemented without compromising the oxidation resistance.
2. Based upon the limited available information in the literature, disilicides, especially $MoSi_2$ do not exhibit stable two-phase equilibria with ductile refractory metals. However, in ternary systems involving boron and silicon a Mo- Mo_5SiB_2 and Nb- Nb_5SiB_2 equilibrium has been reported. In the current work the main features of the phase stability in the Mo-Si-B system have been established at 1600 and 1200°C. This work has confirmed the coexistence of two-phase mixtures of Mo and Mo_5SiB_2 (T_2

phase) as a stable equilibrium at high temperature. Similar initial work on the Nb-Si-B system has also confirmed the existence of a stable Nb + T₂ two phase field.

3. The principal solidification reactions in the Mo-Si-B system have been identified. These reactions feature extensive compositional segregation which is manifested by the formation of boride and silicide phases. Long term, elevated temperature annealing of as-cast structures is not an effective approach to removing the slowly dissolving segregation induced boride and silicide phases.
4. Rapid solidification processing has been applied in the current work to mitigate the problems associated with as-cast segregation. With rapid solidification it has been demonstrated that the segregation induced formation of boride and silicide phases can be suppressed so that Mo(ss) + T₂ two phase mixtures can be formed directly from the melt. Upon elevated temperature annealing the as-cast structure develops into a stable uniform two-phase equiaxed microstructure.
5. The T₂ (Mo₅SiB₂) phase is not a line compound, but exhibits a solubility range of several atomic percent towards Si and B rich values. The Nb₅SiB₂ phase also exhibits a solubility range which is more extensive than that for Mo₅SiB₂. The observation of a solubility range also implies the existence of a defect structure in the T₂ phase in order to accommodate non-stoichiometry.
6. Due to the solubility range a supersaturation can develop in the T₂ phase during solidification. This feature has been exploited in the current work to allow for the development of Mo precipitates within the T₂ phase. The crystallography and interfacial structure associated with the precipitation reaction have been established. The T₂/Mo interface exhibits a high degree of coherency which is reflected in the

remarkable stability of the Mo precipitates to coarsening during elevated temperature exposure. Moreover, the Mo precipitates have been demonstrated to provide an effective toughening enhancement to the T₂ phase. This discovery opens new opportunities for microstructural control.

7. Diffusion couples between binary boride and silicide phases have been successfully constructed to allow for the synthesis of the T₂ phase during interdiffusion. For a couple between Mo₂B and Mo₅Si₃ the observed diffusion path exhibited a transient period before yielding a single phase T₂ product. An analysis of the composition profiles established during interdiffusion yields a diffusivity for the T₂ phase of about 10⁻¹⁵ m²/s at 1600°C.

5) Publication and Presentation

Publication

- 1) Nunes, C. A., Sakidja, R. and Perepezko, J. H., in Structural Intermetallics 1997, edited by M. V. Nathal, R. Darolia, C. T. Liu, P. L. Martin, D. B. Miracle, R. Wagner and M. Yamaguchi, (TMS, Warrendale, PA, 1997), pp.831-839.
- 2) Perepezko, J. H., Nunes, C. A., Yi, S. H. and Thoma, D. J., in High-Temperature Ordered Intermetallic Alloys VII, edited by C.C. Koch, C. T. Liu, N. S. Stoloff and A. Wanner, (Mater. Res. Soc. Proc. 460, Pittsburgh, PA, 1997), pp 1-14.

- 3) Sakidja, R., Sieber, H. and Perepezko, J. H., in Molybdenum and Molybdenum Alloys, edited by A. Crowson, E. S. Chen, J.A Shield and P. R. Subramanian (TMS, Warrendale, PA, 1998), pp. 99-110.
- 4) Sakidja, R., Wilde, G., Sieber, H. and Perepezko, J. H., in High-Temperature Ordered Intermetallic Alloys VIII, edited by E.P. George, M. Yamaguchi, M.J. Mills, MRS Symp. 522, pp. (1999).
- 5) Sakidja, R. Sieber, H. Perepezko, J.H., Philosophical Magazine Letters, **79** [6], pp. 351-357 (1999).
- 6) Nunes, C. A., Sakidja, R., Dong, Z and Perepezko, J. H., "Liquidus Projection for the Mo-rich portion of the Mo-Si-B ternary system, Intermetallics (1999) in press.

Conferences/Presentations

- 1) The first four publications (1-4) were published in the proceedings of the respective conferences and involved presentations as well.
- 2) Perepezko, J. H., Sakidja, R. and Nunes, C. A., "Alloy Designs for High Temperature Applications in the Mo-Si-B System", presented at AEROMAT '98 in Tysons Corner, VA (June 15-18, 1998).
- 3) Perepezko, J. H., Sakidja, R. and Nunes, C. A. "Phase Stability in Mo-Si-B Alloys", presented at High Temperature Materials Workshop, WPAFB (Oct. 15-16, 1997).
- 4) Myers, J. and Sakidja, R., "Understanding the Processing of High Temperature Intermetallics through Phase Equilibria: A study of the Mo-Si-B and Nb-Si-B

- systems”, presented at the 1998 Wisconsin Space Conference in Ripon, WI (August 14, 1998).
- 5) Perepezko, J. H., Sakidja, R., Myers, J. and Kim, S., “Microstructural Designs in High-Temperature (Mo,Nb)-Si-B Alloys, “ presented at the TMS 1999 Annual Meeting in San Francisco, CA.
 - 6) Perepezko, J. H., Sakidja, R., Kim, S., Myers, J. and Sieber, H., “Phase Stability and Microstructure Control in High-Temperature Mo-Si-B System”, *US/Japan Workshop on Very High Temperature Structural Materials* .

6. References

- [99Dan] DAYANANDA, M.A. and SOHN, Y.H., Metall. Mater. Trans. A, 30A: 535, 1999
- [99Kim] KIM, S., unpublished work, 1999.
- [99Mey] MEYER, M.K., THOM, A.J. and AKINC, M., Intermetallics, 7, p153, 1999
- [98Hua] HUANG, W. and CHANG, Y.A., Intermetallics, 6, 487, 1998
- [97Ans] ANSARA, I., DUPIN, N., LUKAS, H.L. and SUNDMAN, B., J. Alloys and Comp., 247, 20, 1997
- [97Nun] NUNES, C.A., SAKIDJA, R. and PEREPEZKO, J.H., in Structural Intermetallics 1997 (edited by Nathal, M.V., Darolia, R., Liu, C.T., Martin, P.L., Miracle, D.B., Wagner, R. and Yamaguchi, M.), 831, 1997
- [97Per] PEREPEZKO, J. H., NUNES, C. A., YI, S. H. AND THOMA, D. J., in *High-Temperature Ordered Intermetallic Alloys VII*, edited by C.C. Koch, C. T. Liu, N. S. Stoloff and A. Wanner, Mater. Res. Soc. Symp. Proc. 460: 1-14, 1997
- [96Kim] KIM, S., Ph.D. thesis, University of Wisconsin – Madison, USA, 1996

- [96Jac] JACKSON, M. R., BEWLAY, B. P., ROWE, R. G., SKELLY, D. W., LIPSITT, H. A., JOM 48 , p. 39, 1996
- [96Mey] MEYER, M. K. AND AKINC, M., J. Am. Ceram. Soc., 79(4), p938, 1996
- [96Ros] ROSSOUW, C. J., FORWOOD, C. T., GIBSON, M. A. and MILLER, P. R., Phil. Mag. A, 74, 57, 1996 & 74, 77, 1996
- [94Cha] K. S. CHAN, in Intermetallic Matrix Composites III, edited by J. A. Graves, R. R. Bowman, J. J. Lewandowski, (Mater. Res. Soc. Proc. 364, Pittsburgh, PA, 1994), pp. 469-480.
- [93Cam] CAMECA. Quantiview 3.0 Reference Guide. Overlapping Correction Program (FILOVL Program): 16.1 - 16.6. Courbevoie Cedex (France), 1993
- [92Asm] ASM HANDBOOK Vol 3 ALLOY PHASE DIAGRAMS, ASM International, Ohio, USA, 1992
- [92Ber] BERZTISS, D. A., CERCHIARA, R. R., GULBRANSEN, E. A., PETTI, F. S. and MEIER, G. H. Materials. Materials Science and Engineering. A155: 165, 1992
- [92Boe] BOETTINGER, W., PEREPEZKO, J. H. and FRANKWICZ, P. S. Materials. Materials Science and Engineering. A155: 33, 1992
- [92Cho] CHOU, T. C. and NIEH, T.G. Scripta Metallurgica et Materialia. 26: 1637, 1992
- [92Coo] COOK, J., KHAN, A.; LEE, E. and MAHAPATRA, R. Materials Science and Engineering. A155: 183-198, 1992
- [92Dim] DIMIDUK, D. M., MIRACLE, D. B. and WARD, C. H. Materials Science and Technology. 8: 367, 1992
- [92Kub] KUBASCHEWSKI, O., ALCOCK, C.B. and Spencer, P.J., Materials Thermochemistry 6th edition, Pergamon Press, Oxford, UK, 1992.
- [92Uz] UZ, M.. & WITTENAUER, J. P. Journal of Metals. 44: 25, 1992
- [92Mes] MESCHTER, P.J. Metallurgical Transactions A. 23A: 1763, 1992
- [92Mue] MUELLER, A., WANG, G., RAPP, R.A. and COURTRIGHT, E.L. Journal. Electrochem. Soc. 139 (5) : 1266, 1992
- [92Sha] SHAH, D. M., BERZIK, D., ANTON, D. L. and HECHT, R. Mat. Sci. Eng. A155: 45, 1992

- [92Vas] VASUDÉVAN, A. K. & PETROVIC, J. J. *Materials Science and Engineering*. A155 : 1, 1992
- [91Daa] DAAMS, J.L.C., VILLARS, P. and Van Vucht, J.H.N. *Atlas of Crystal Structures Types for Intermetallic Phases*. ASM. Metals Park, Ohio. p.4296-4299, 1991
- [91Dev] DEVE, H.E. AND MALONEY, M. J., *Acta metall. Mater.*, 39 [10] (1991) pp. 2275-2284
- [91Eva] EVANS, A.G. *Materials Science and Engineering*. A143: 63, 1991
- [91Kim] KIM, Y.W. & DIMIDUK, D.M. *Journal of Metals*. 43: 40, 1991
- [91Per] PEREPEZKO, J. H. *ISIJ International*. 31(10): 1080, 1991
- [91Xia] XIAO, L.; KIM, Y.S.; ABBASCHIAN and HECHT, R.J. *Materials Science and Engineering*. A144: 277, 1991
- [90Mas] MASSALSKI, T.B. *Binary Alloy Phase Diagrams*. American Society for Metals. Metals Park, Ohio. v.1: 502,503; v.3: 2664,2666, 1990
- [90Wit] WITTENAUER, J. *Journal of Metals*. 42 : 7, 1990
- [89Des] DESTEFANI, J.D. *Advanced Materials and Processes*. (2) : 37, 1989
- [89Mat] MATAGA, P.A. *Acta Met.* 37: 3349, 1989
- [88Buc] BUCKMAN, R.W. in *Alloying*. Chapter 12, p. 419. Edited by John L. Walter, Melvin R. Jackson and Chester T. Sims. ASM. Metals Park, Ohio, 1988
- [88Pen] PENNYCOOK, S.J., *Ultramicroscopy*, 26, 239, 1988
- [88Tho] THOULESS, M.D. & EVANS, A.G. 36 : 517, 1988
- [88Via] VIARS, P.R. Report #AIAA-892137, American Institute of Aeronautics and Astronautics, Systems and Operation Conf. Seattle, WA. 31 July - 2 August, 1988
- [87JCP] JCPDS. *Powder Diffraction File*. International Centre for Diffraction Data. Swarthmore, PA. Card # 9-292, 1987
- [87Kir] KIRKALDY, J.S. and YOUNG, D.J., *Diffusion in the Condensed State*, The Institute of Metals, 199-272, 1987
- [86Hep] HEPPEHEIMER, T.A. *High Technology*. 7 : 46, 1986
- [85Fle] FLEISCHER, R.L. *Journal of Metals*. 37 : 16 (1985)
- [84Hor] HORNBOGEN, E. *Acta Met.* 32: 615, 1984

- [83Bir] Birks, N. and Meier, G. H., "Introduction to High Temperature Oxidation of Metals" (Edward Arnold, London) 54, 1983.
- [83Smi] Smithells Metals Reference Book 6th edition (ed. Brandes, E. A.), Butterworths, 13-11, 1983
- [83Spe] SPENCE, J.C.H. and TAFT, J., J. Microscopy, 130, 147, 1983
- [82Gru] GRUNLING, H.W. & BAUER, R. Thin Solid Films. 95: 3, 1982.
- [81Sun] SUNDAMAN, B. and AGREN, J., J. Phys. Chem. Solids, 42, 297, 1981
- [79Mei] MEIER, K.; MEHRER, H. and REIN, G. Z. Metallk. 70: 271, 1979
- [78Aar] AARONSON, H. I., LEE, J. K. AND RUSSELL, K. C., in *Precipitation Processes in Solids*, edited by K. C. Russell and H. I. Aaronson (The Metallurgical Society of AIME, Warrendale, PA, 1978) pp. 31-85
- [78Sch] SCHLICHTING, J. High Temperature -High Press. 10 : 241, 1978
- [76Koc] KOCHERZHINSKII, Y.A. & KULIK, O.G. Metallofizika. 64 : 44, 1976
- [72GUL] E. A. GULBRANSEN AND S. A. JANSSON, Oxidation of Metals, 4(3): 181, 1972
- [70Hil] HILLERT, M and STAFFANSON, L.-I., Acta Chem. Scand., 24, 3618, 1970
- [68Sne] SNETSINGER, K.G., BUNCH, T.E and KEIL, K., American Mineralogist, 53: 1770, 1968
- [67Gol] GOLDSCHMIDT, H.J. Interstitial Alloys. Plenum Press. New York, 1967
- [67Sko] SKOLOZDRA, R.V. & GLADYSHEVSKII, E.I. Visn. L'viv. Derzh. Univ. Ser. Khim. 9: 21, 1967
- [65Bar] R. W. Bartlett, J. W. McCamont and P. R. Gage, J. Am. Ceram. Soc., 48(11): 551, 1965
- [65Ber] J. B. Berkowitz-Mattuck and R. R. Dils, J. Electrochem. Soc., 112(6) : 583, 1965
- [65Sav] SAVITSKIY, E. M., BARON, V. V., BYCHKOVA, M. I., BAKUTA, S. A., GLADYSHEVSKIY, E. I., Russian Metallurgy, translated from Izvestiya Akademii Nauk SSSR, Metally, 2: 91-96, 1965.
- [65Wag] WAGNER, C. Corrosion Science. 5: 751, 1965

- [64Bar] R. W. BARTLETT, P. R. GAGE AND P. A. LARSSEN, Trans AIME, 230: 1528, 1964.
- [60Aro] ARONSSON, B. Acta Chem. Scand. 14 : 1414, 1960
- [60Now] NOWOTNY, H.; BENESOVSKY, F.; RUDY, E. and WITTMANN, A. Monatshefte Fuer Chemie. 91 : 975, 1960
- [59Wag] WAGNER, C. Z. Elektrochem. 63 : 772, 1959
- [58Aro] ARONSON, B. Acta Chemica Scandinavica. 12 (1) : 31, 1958
- [58Pug] PUGH, J. Journal of Metals. 212 : 340, 1958
- [57Now] NOWOTNY, H., KIEFFER, R., BENESOVSKY, F. Planseeberichte Fuer Pulvermetallurgie, 5 : 86, 1957
- [56Fuj] H. FUJITA AND L. J. Gosting, J. Am. Chem. Soc., 78, p1099, 1956
- [55Aro] ARONSON, B. Acta Chemica Scandinavica. 9: 1107, 1955
- [54Now] NOWOTNY, H., PARTHE, E., KIEFFER, R. AND BENESOVSKY, F., Monatshefte Fuer Chemie., 85 : 255, 1954
- [42Sch] SCHEIL, E. Z. Metallk. 34 : 70, 1942
- [45Tem] TEMKIN, M., Acta Phys. Chim., 20, 411, 1945 [31Ons] ONSAGER, L., Phys. Rev., 37, 405, 1931
- [32Ons] ONSAGER, L., Phys. Rev., 38, 2265, 1932

7 Appendix

In general, the interdiffusion process plays major role in microstructure control such as solid state transformation or precipitation process. Onsager's formalism [31Ons, 32Ons] described the interdiffusion behavior of various components based on $(n-1)^2$ interdiffusion coefficients in an n -component system. The problem is that multiple diffusion couples with crossing diffusion paths must be prepared in order to obtain the diffusivities at the composition of the crossing point. Since there are four independent interdiffusion coefficients in 3-component system [87Kir], the Fick's law is

$$J_i = -\sum_j^2 D_{ij}^3 \frac{\partial C_j}{\partial x} \quad (i, j = 1 \text{ or } 2).$$

where J_i is the interdiffusion flux of component i , $\frac{\partial C_i}{\partial x}$ is the concentration gradient of i and D_{ij}^3 is the interdiffusion coefficient being defined as the ratio of the net number of i atoms moving between two planes to the negative concentration gradient of j between those planes. Component 1 and 2 are selected as independent, and the superscript '3' is used in D_{ij}^3 . There exist 4 unknown interdiffusion coefficients and only two known relations in a single concentration profile. If two diffusion couples cross diffusion paths, the 4 unknown interdiffusion coefficients can be found from the four known relations at the crossing point. However, a new analysis method determining ternary interdiffusion coefficients from a single diffusion couple has been developed by Kim [99Kim], based on the linear regression method solving n linear equations with m unknown variables ($n < m$). Since his model was established under an assumption of concentration-independent interdiffusion coefficients, the model can be applied in a diffusion couple containing small concentration differences.

Smoothed lines for Si and B can be obtained from raw data of concentration profiles using the polynomial equation and the curve fitting method. Using the following relation

$$J_i = \frac{1}{2t} \int_{C_i^{+\infty}}^{C_i(x)} (x - x_0) dC_i \quad \text{where } x_0 \text{ is the place where } \int_{C_i^{+\infty}}^{C_i^{-\infty}} (x - x_0) dC_i = 0$$

the interdiffusion flux of Si and B respectively is estimated. x_0 represents the position of the Matano plane and t is the annealing time. If the T_2 phase region is divided into l small

intervals, then, from smoothed lines, it is possible to estimate the interdiffusion flux

$((J_i)_{x=x_k})$ and the concentration gradient $\left(\frac{\partial C_j}{\partial x}\right)_{x=x_k}$ at $x=x_k$ ($k = 0, 1, 2 \dots l$). Defining

$$X(k) = \left(\frac{\partial C_1}{\partial x}\right)_{x=x_k}, \quad Y(k) = \left(\frac{\partial C_2}{\partial x}\right)_{x=x_k}, \quad Z(k) = (J_i)_{x=x_k}$$

and using the least square method, the interdiffusion coefficients becomes

$$D_{i1}^3 = -\frac{\begin{vmatrix} \sum_k X(k)Z(k) & \sum_k X(k)Y(k) \\ \sum_k Y(k)Z(k) & \sum_k Y(k)Y(k) \end{vmatrix}}{\begin{vmatrix} \sum_k X(k)X(k) & \sum_k X(k)Y(k) \\ \sum_k Y(k)X(k) & \sum_k Y(k)Y(k) \end{vmatrix}} \quad \text{and} \quad D_{i2}^3 = -\frac{\begin{vmatrix} \sum_k X(k)X(k) & \sum_k X(k)Z(k) \\ \sum_k Y(k)X(k) & \sum_k Y(k)Z(k) \end{vmatrix}}{\begin{vmatrix} \sum_k X(k)X(k) & \sum_k X(k)Y(k) \\ \sum_k Y(k)X(k) & \sum_k Y(k)Y(k) \end{vmatrix}}$$

8) Tables

Table 1 - The Thermodynamic Data of Phases in the Mo-Si and Mo-B Binary Systems [KUB]

Phase	S_{298} (J/deg·mol)	$-\Delta H_{298}$ (KJ/mol)	C_p (J/K·mol)
B	5.9	0.0	$17.91 + 9.64 \times 10^{-3} T - 8.58 \times 10^5 T^{-2} - 1.80 \times 10^{-6} T^2$
Mo	28.6	0.0	$28.52 - 4.42 \times 10^{-3} T - 3.62 \times 10^5 T^{-2} + 4.28 \times 10^{-6} T^2$
Mo ₂ B	52.6±8.4	132.2±25.1	$78.45 + 4.56 \times 10^{-3} T - 19.37 \times 10^5 T^{-2} + 2.80 \times 10^{-6} T^2$
MoB	25.3±8.4	123.8±16.7	$45.40 + 5.82 \times 10^{-3} T - 13.05 \times 10^5 T^{-2}$
Mo ₃ Si	106.3±1.3	116.3±9.2	$85.86 + 22.68 \times 10^{-3} T + 0.32 \times 10^5 T^{-2}$
Mo ₅ Si ₃	207.9±9.2	310.0±22.2	$183.34 + 35.02 \times 10^{-3} T - 12.01 \times 10^5 T^{-2}$
MoSi ₂	65.1±3.8	131.8±8.4	$67.86 + 11.97 \times 10^{-3} T - 6.57 \times 10^5 T^{-2}$
Si	18.8	0.0	$23.93 + 2.22 \times 10^{-3} T - 4.14 \times 10^5 T^{-2}$ (solid)
			27.20 (liquid, $\Delta H_f = 50.2$ KJ/mol at 1685K)

Table 2 - The Estimated Free Energy of Formation at 1600°C

Phase	ΔG_f (KJ/mol)	Δg_f (KJ/g-mol)
B	-48.23	-48.23
Mo	-103.03	-103.03
Mo ₂ B	-371.33	-123.78
MoB	-253.48	-126.74
Mo ₃ Si	-504.15	-126.04
Mo ₅ Si ₃	-1076.35	-134.54
MoSi ₂	-390.44	-130.15
Si	-85.18	-85.18

Table 3- The Estimated Free Energy of Formation of T₂

Temperature		Free Energy of Formation (KJ/mole)
(°C)	(K)	
1200	1473	-845.39 ± 6.72
1300	1573	-893.70 ± 6.42
1400	1673	-943.50 ± 6.08
1500	1773	-994.72 ± 5.70
1600	1873	-1047.30 ± 5.29

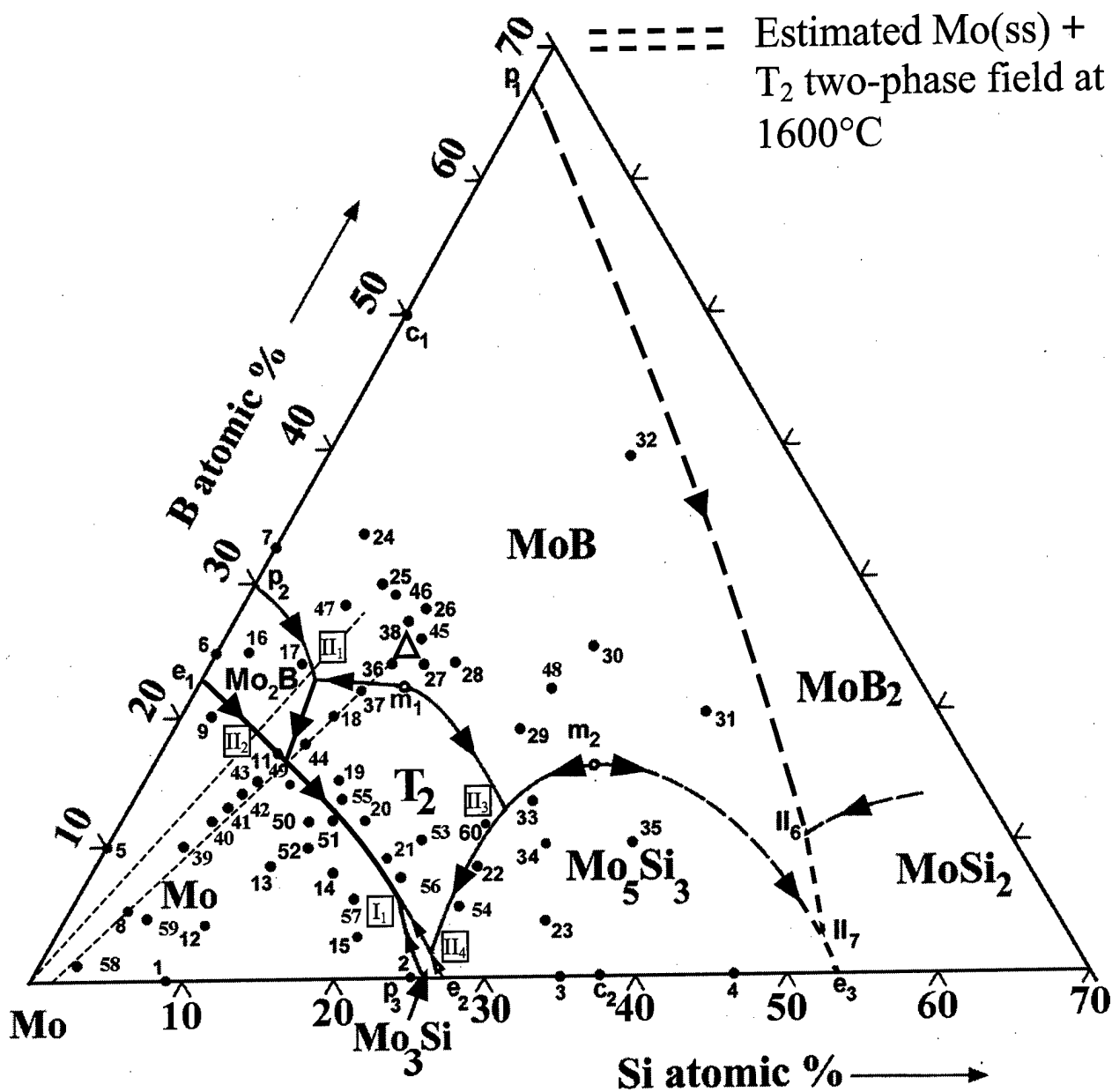


Figure 1: The liquidus projection on the Mo-rich portion of Mo-Si-B ternary system. The region bordered by the dotted lines represents the the estimated location of Mo(ss) + T₂ two-phase field at 1600°C. The triangle point represents the stoichiometric T₂ phase composition.

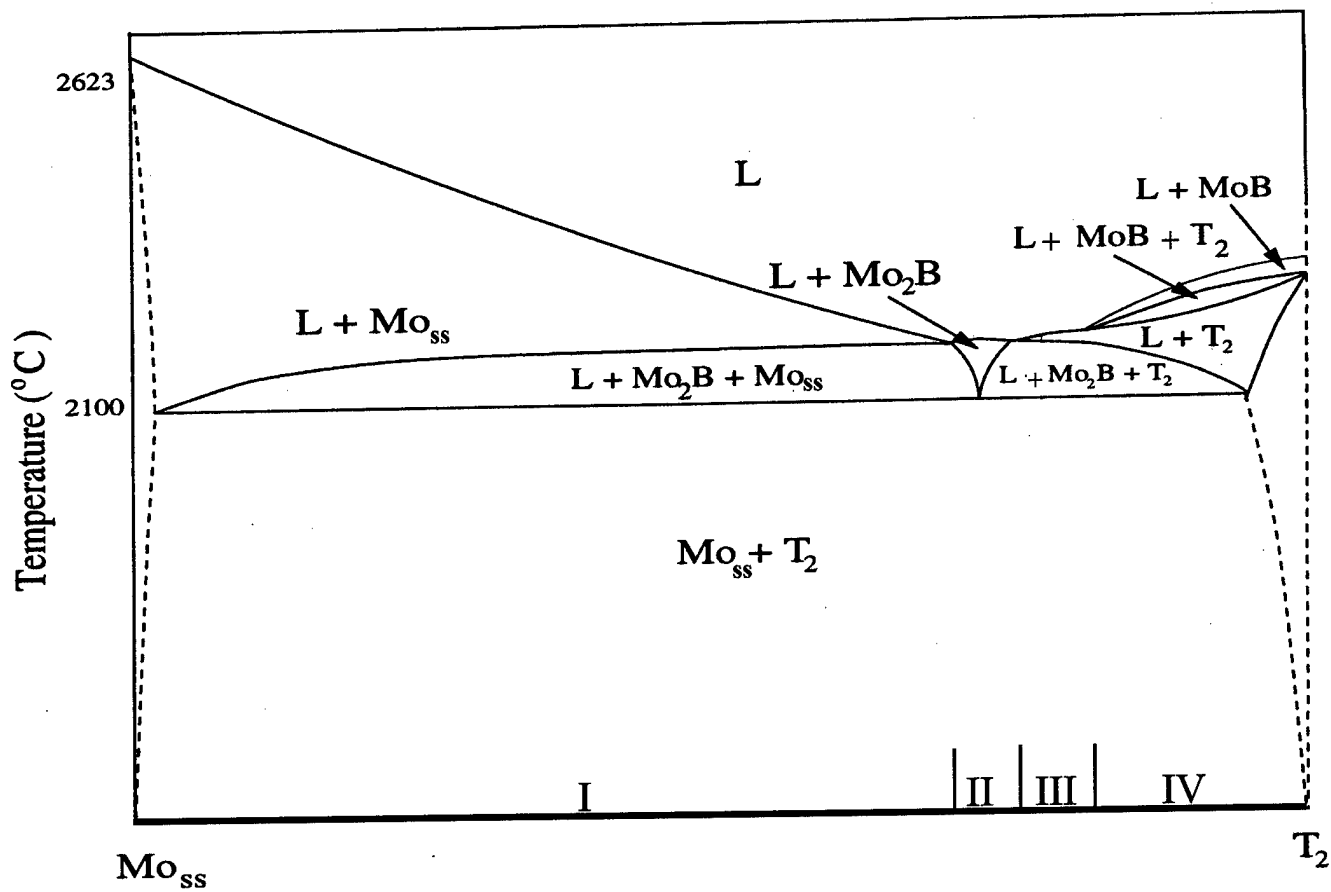


Figure 2 Mo(ss) + T₂ plethal section showing four types of primary solidification

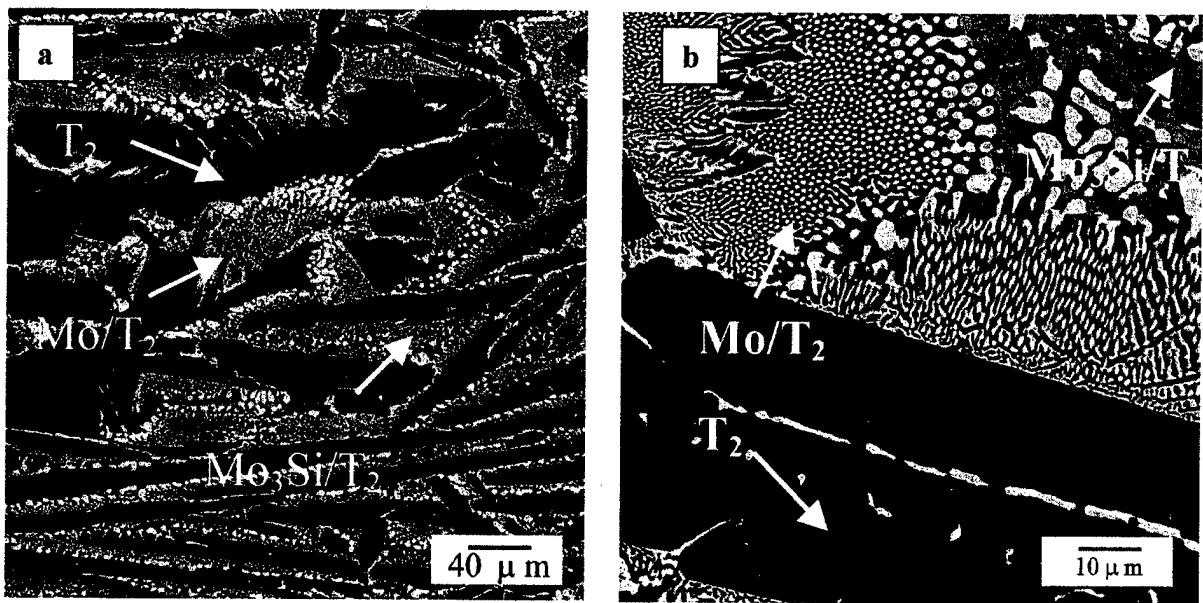


Figure 3 BSE image: **a)** overview of the $\text{Mo}_{70}\text{B}_{20}\text{Si}_{10}$ alloy microstructure as-cast sample, **b)** the same sample at larger magnification.

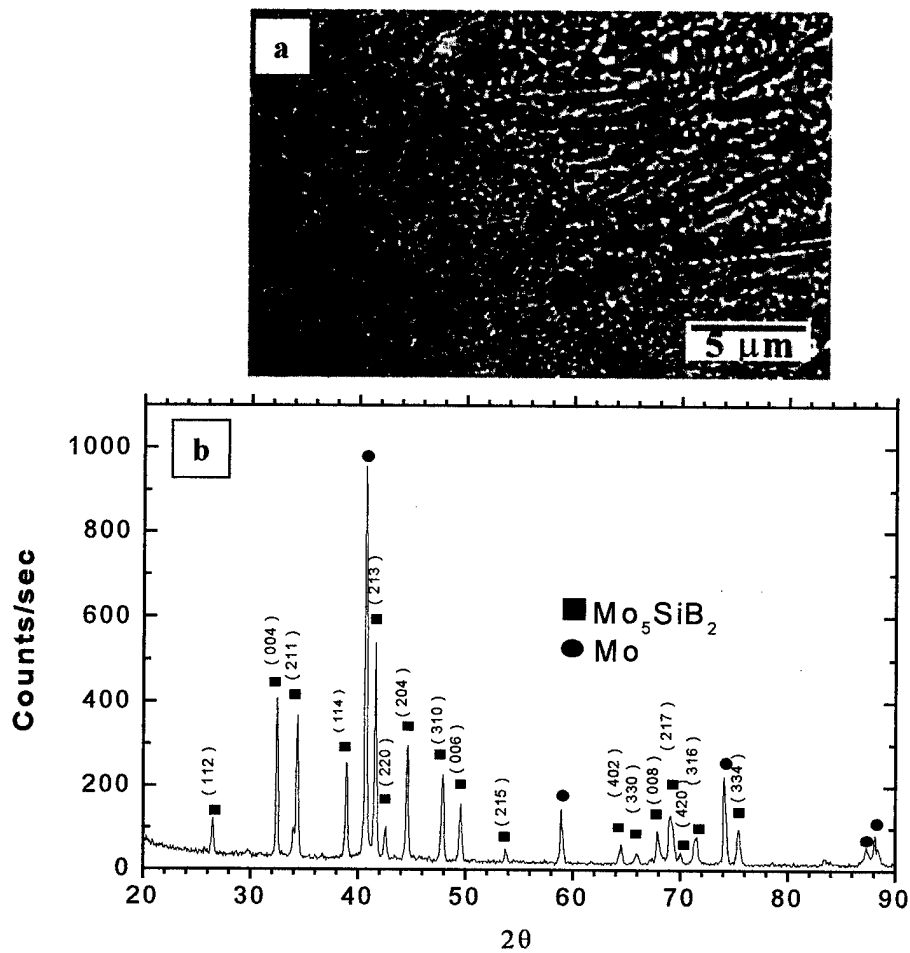


Figure 4 **a)** BSE image of $\text{Mo}_{70}\text{B}_{20}\text{Si}_{10}$ splat, **b)** XRD traces of the splat consisting of Mo and T_2 peaks only.

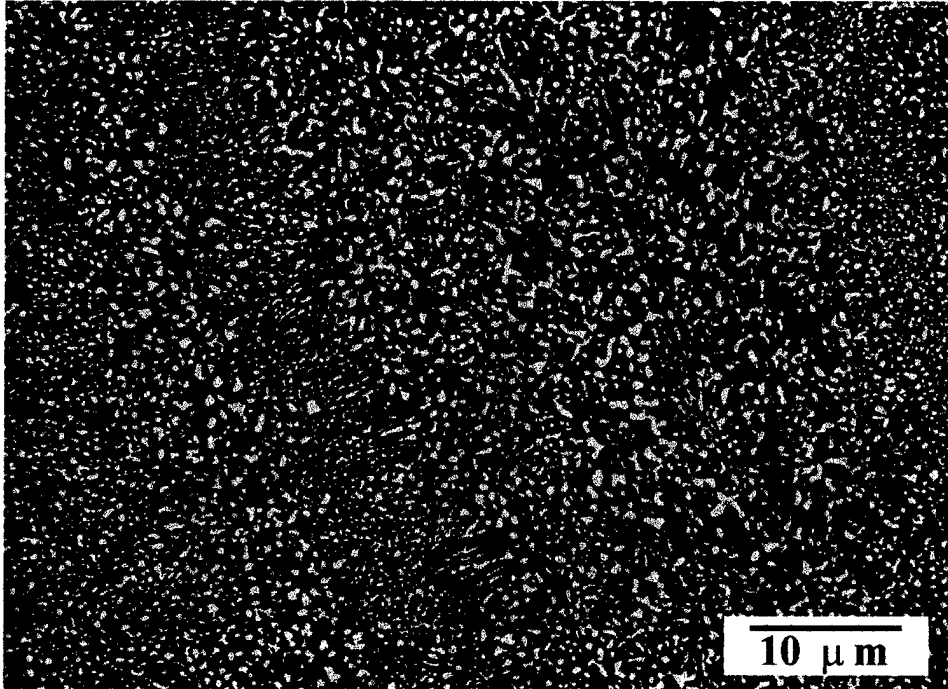


Figure 5 BSE cross-section image $\text{Mo}_{70}\text{B}_{20}\text{Si}_{10}$ SQ foil annealed at 1200°C for 150 hours

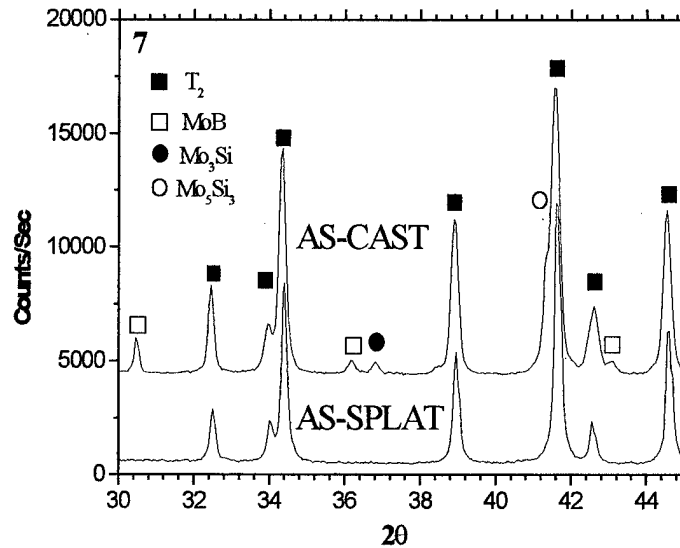
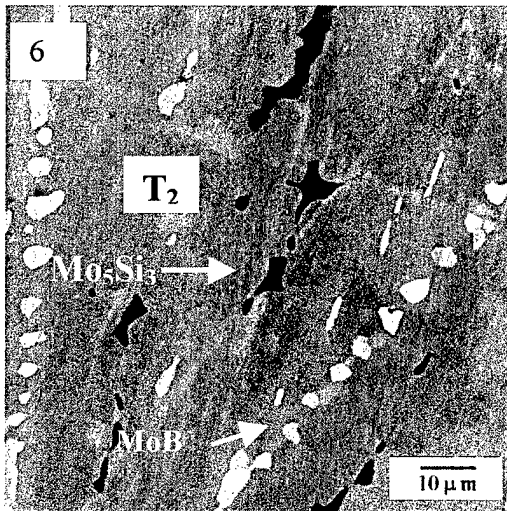


Figure 6 BSE image of $\text{Mo}_{62.5}\text{B}_{25}\text{Si}_{12.5}$ alloys, arc-melted and heat treated at 1600°C for 150 hours

Figure 7 XRD comparison of (1) as-cast $\text{Mo}_{62.5}\text{B}_{25}\text{Si}_{12.5}$ alloys and (2) as-splat $\text{Mo}_{62.5}\text{B}_{25}\text{Si}_{12.5}$

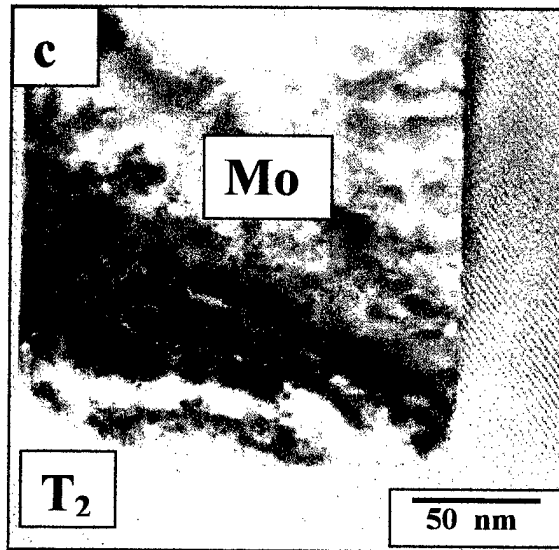
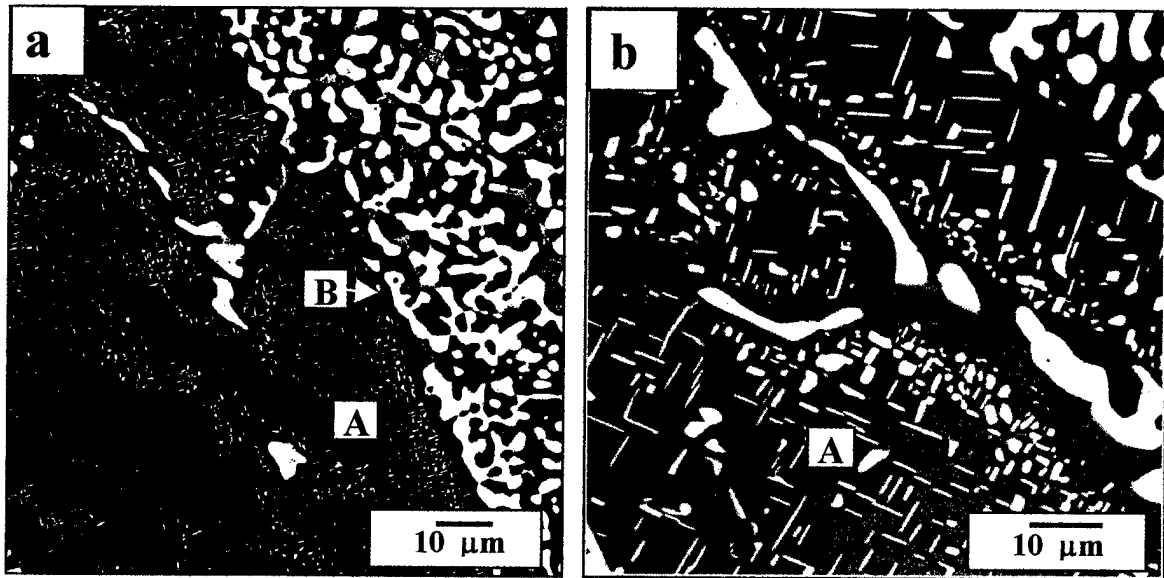


Figure 8 a) BSE image of $\text{Mo}_{70}\text{B}_{20}\text{Si}_{10}$ alloy microstructure after annealing treatment at 1600°C for 25 hours, b) 150 hours, c) TEM bright field image of Mo precipitate within the T_2 matrix;

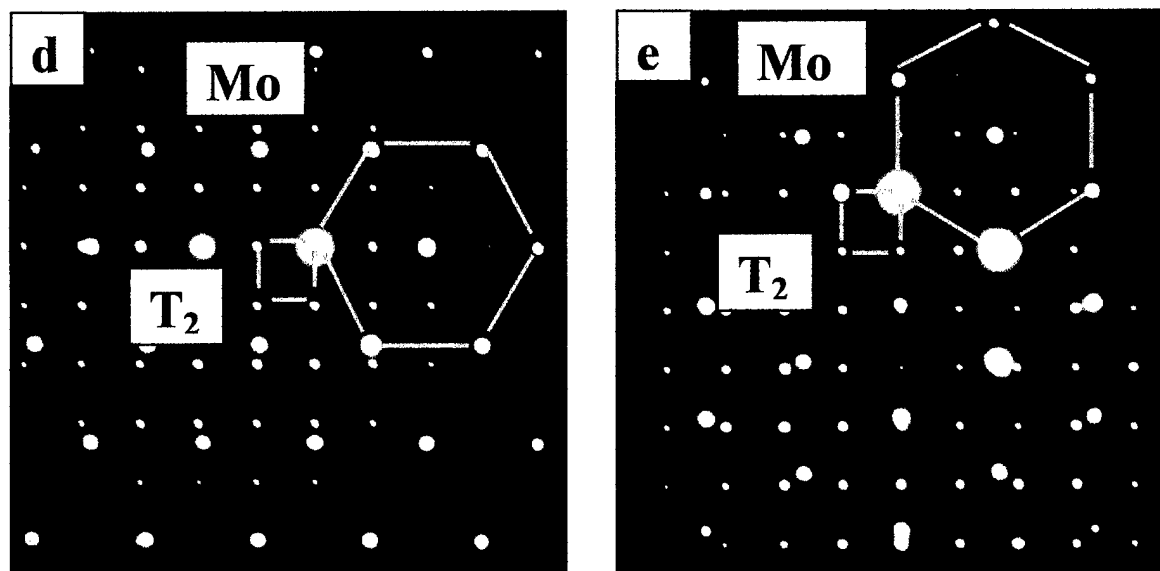


Figure 8 Selected area diffraction pattern (SADP) of Mo/T₂ interface: **d)** Mo {111} || T₂ (001) ; Mo [011] || T₂ [110], **e)** Mo {111} || T₂ (001) ; Mo [011] || T₂ [110].

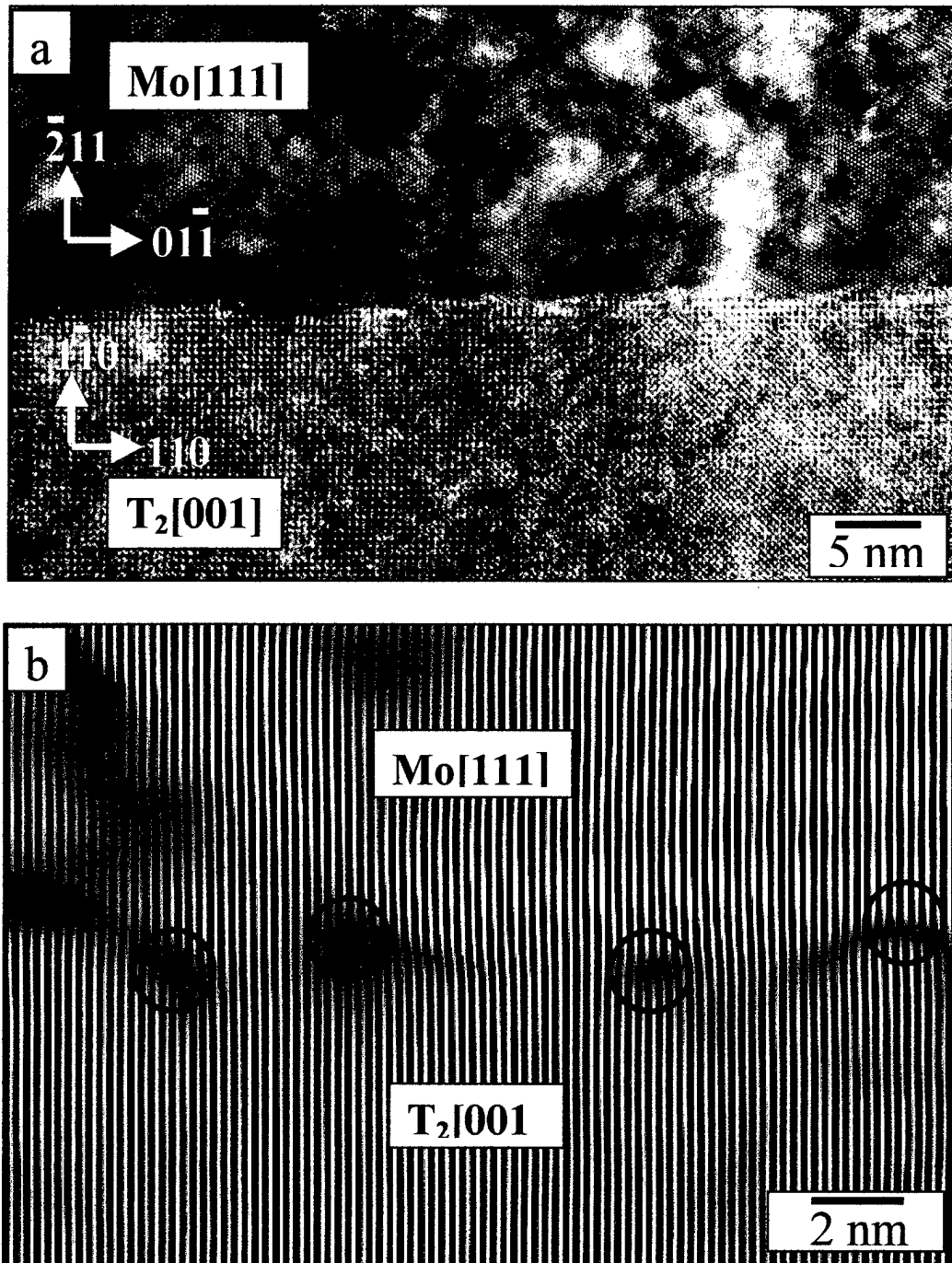


Figure 9:

a) HRTEM image of the long interface of a plate-like Mo precipitate within the T₂ matrix with an orientation following eq. (1a).

b) Fourier-filtered image of a section of the HRTEM micrograph in a) showing a semi-coherent interface. The Fourier-filtering with the Mo (00 $\bar{1}$)/(000) and the T₂ (220)/(000) reflections displays the T₂ (220) extra planes ending at the interfacial dislocations (marked by circles).

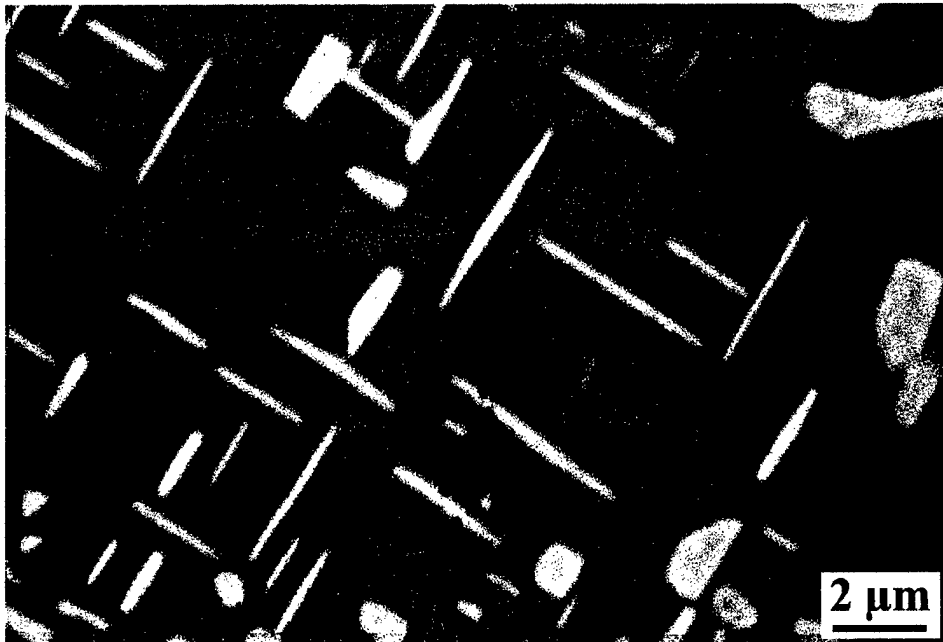


Figure 10a Crack-bridging in a T_2 matrix by Mo(ss) precipitates

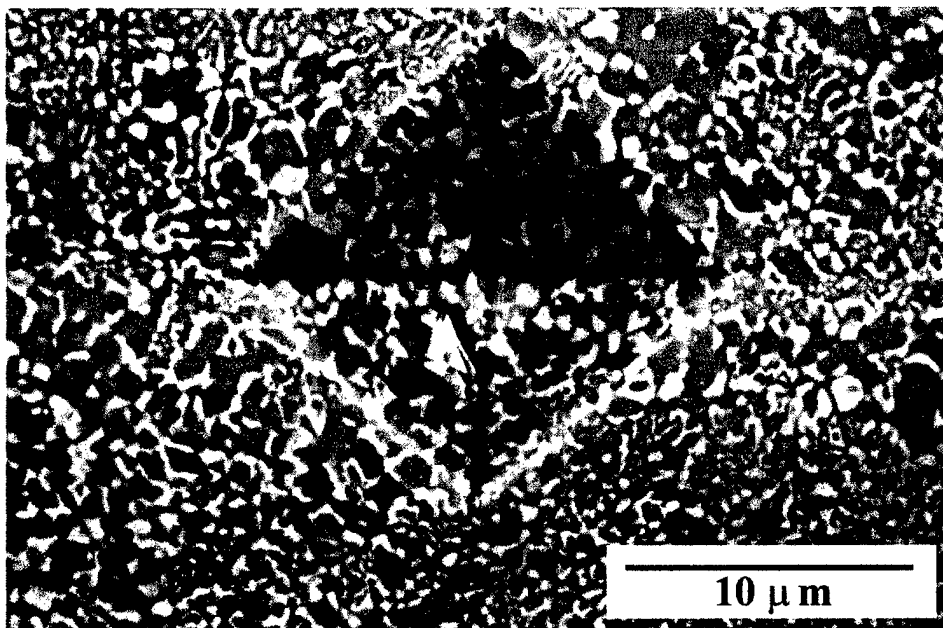


Figure 10b Vickers indentation on Mo-20B-10Si splat-quenched alloys. An enhanced crack growth resistance due to ductile phase toughening is clearly evident.

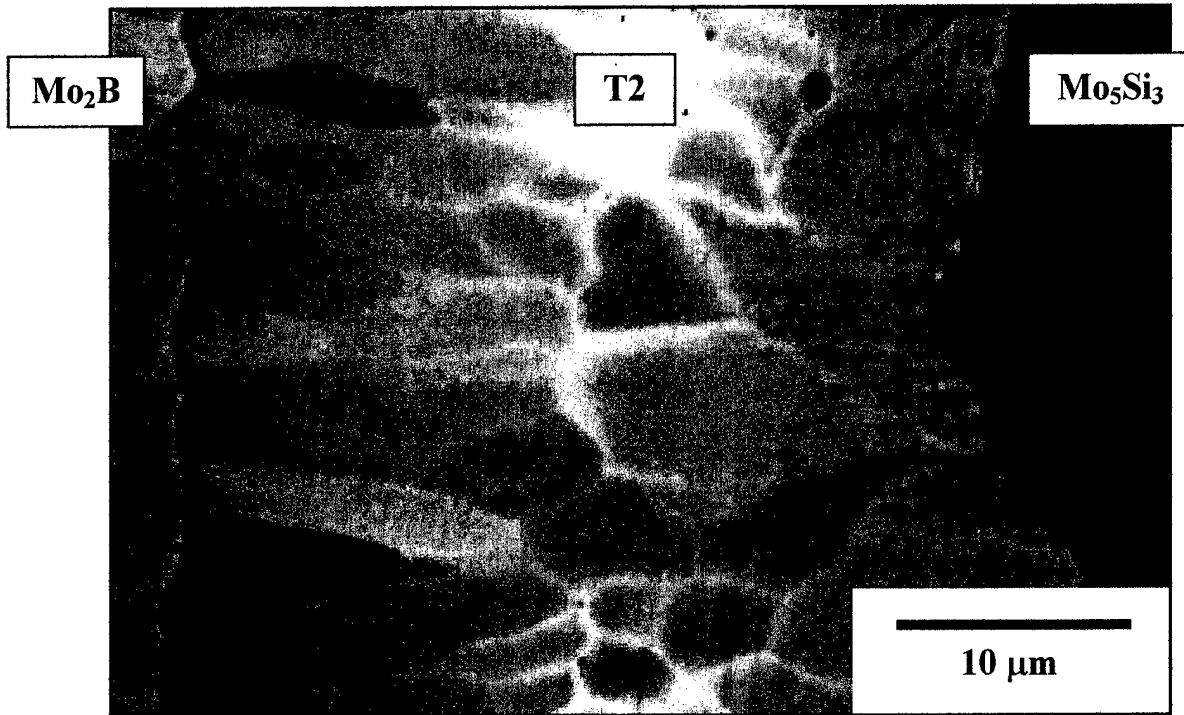
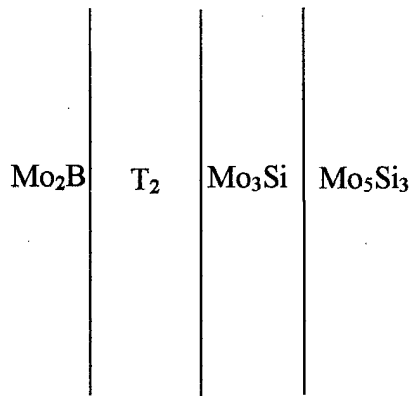
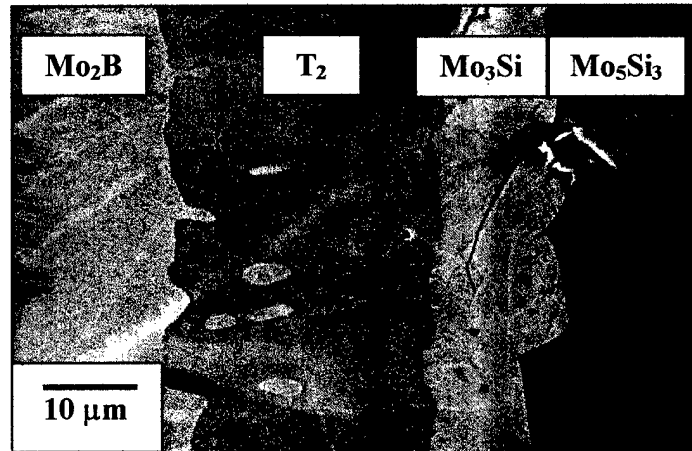


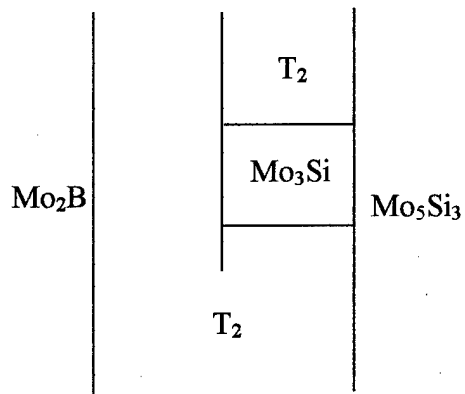
Figure 11- BSE images of the cross-section of diffusion couples annealed at 1600°C for 400 hours



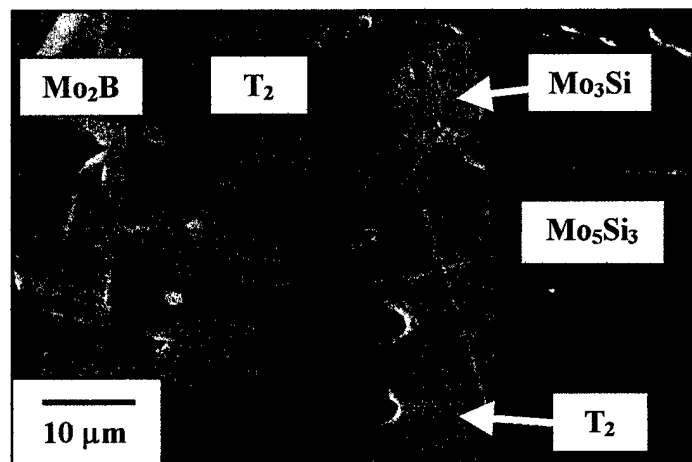
(a)



(b)



(c)



(d)

Figure 12 - The Mo₃Si Phase Existing (a)&(b) along the T₂ Phase and (c)&(d) Partially between the T₂ and the Mo₅Si₃ Phases in the Mo₂B/Mo₅Si₃ Diffusion Couple annealed at 1700°C for 182 hours.

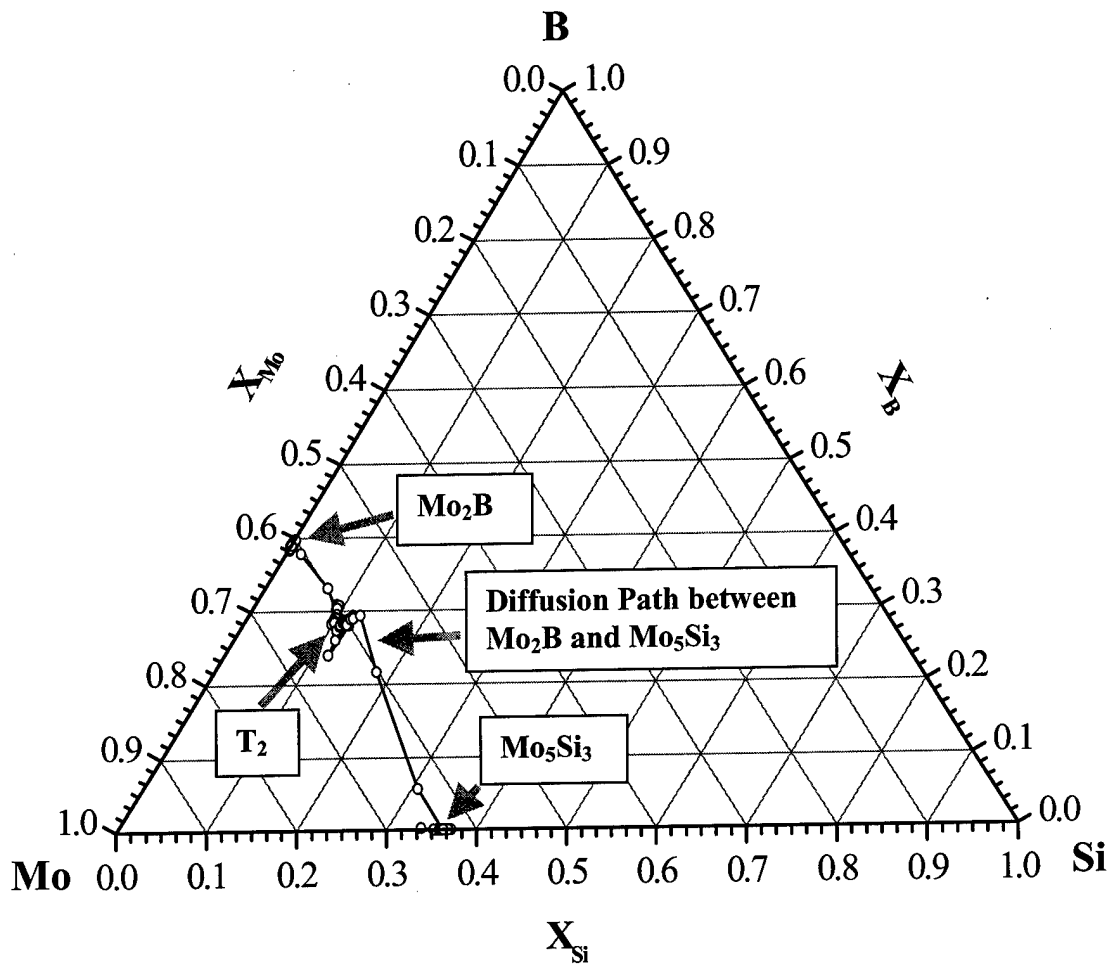


Figure 13 - Diffusion pathway between Mo_2B and Mo_5Si_3 on the isothermal ternary phase diagram

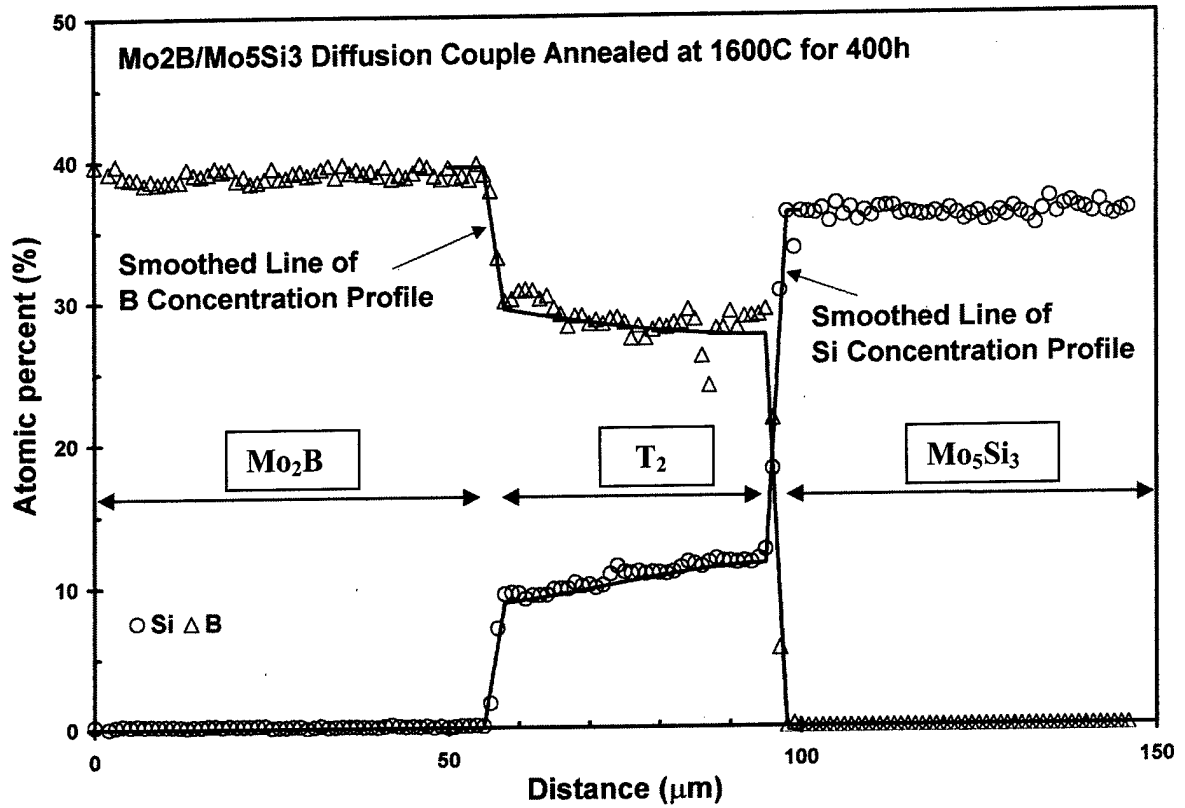


Figure 14 - Concentration profiles of Si and B curve-fitted using the polynomial equations

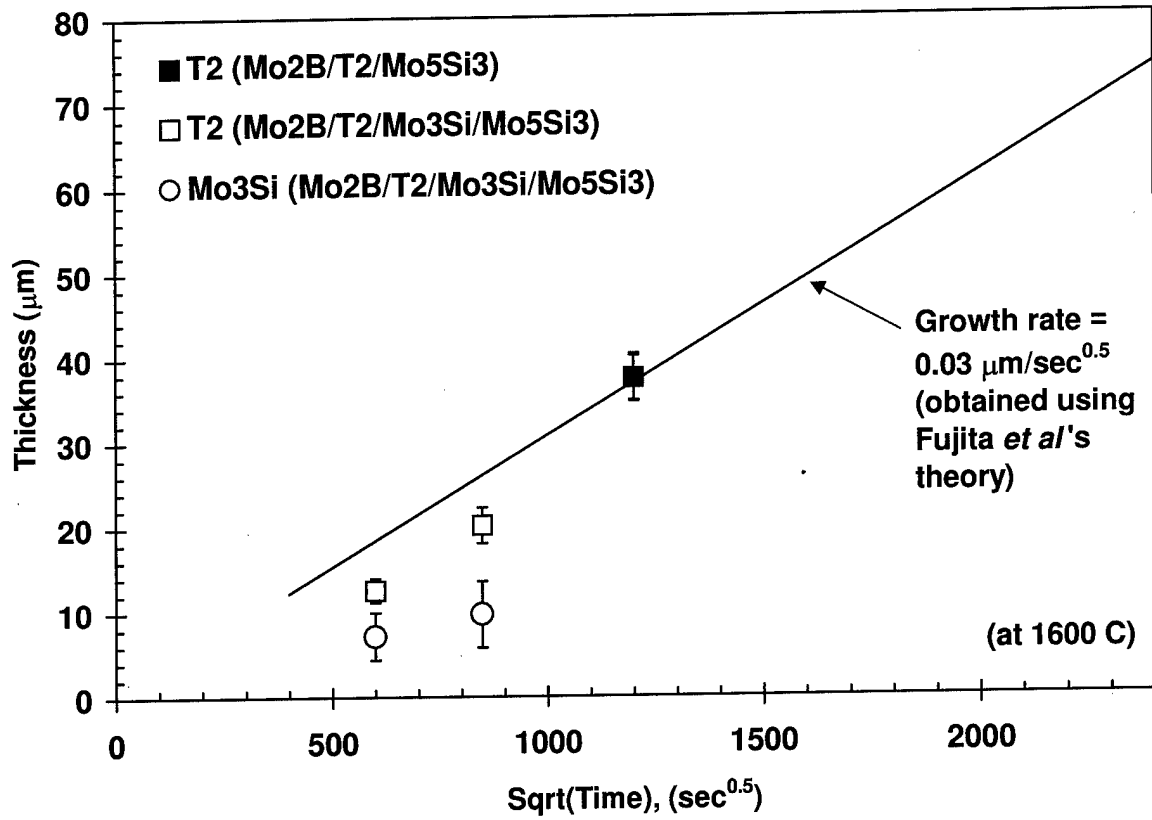


Figure 15 - Plot of growth thickness of the T₂ phase vs square-root time.

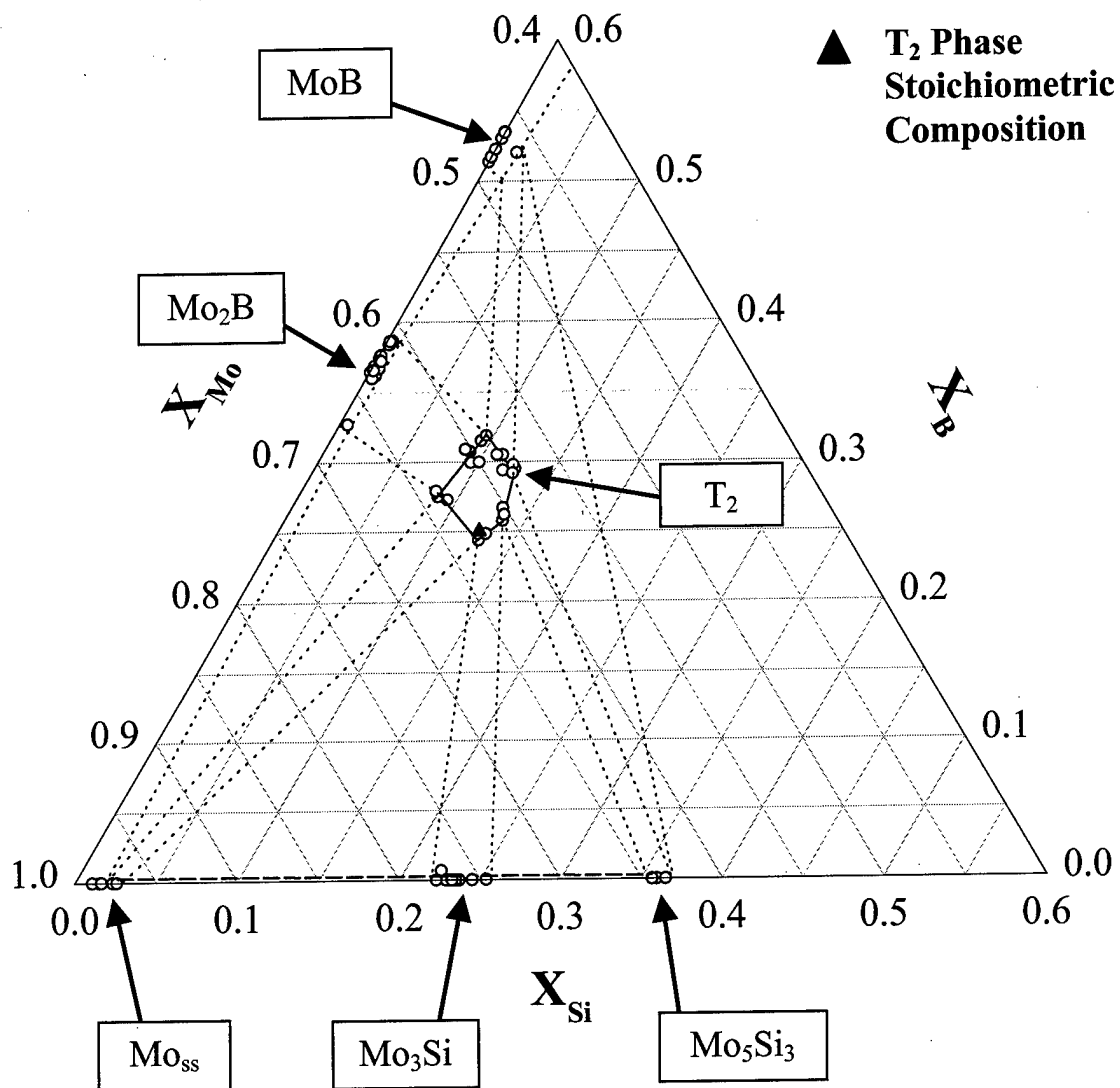


Figure 16 The ternary isothermal section of the Mo-rich Mo-Si-B system showing the phase boundaries.

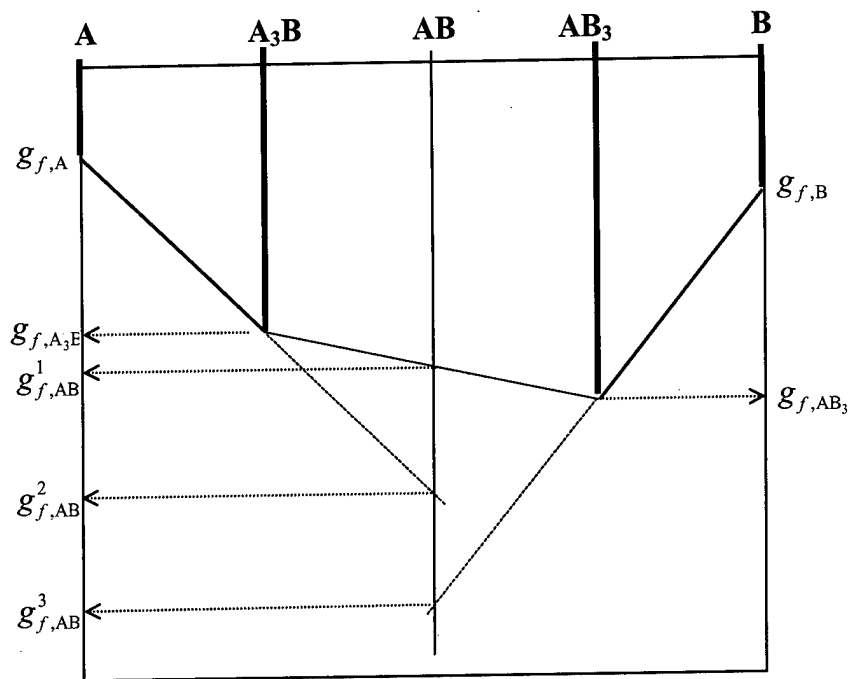


Figure 17 - Schematic Free Energy Diagram in the A-B System

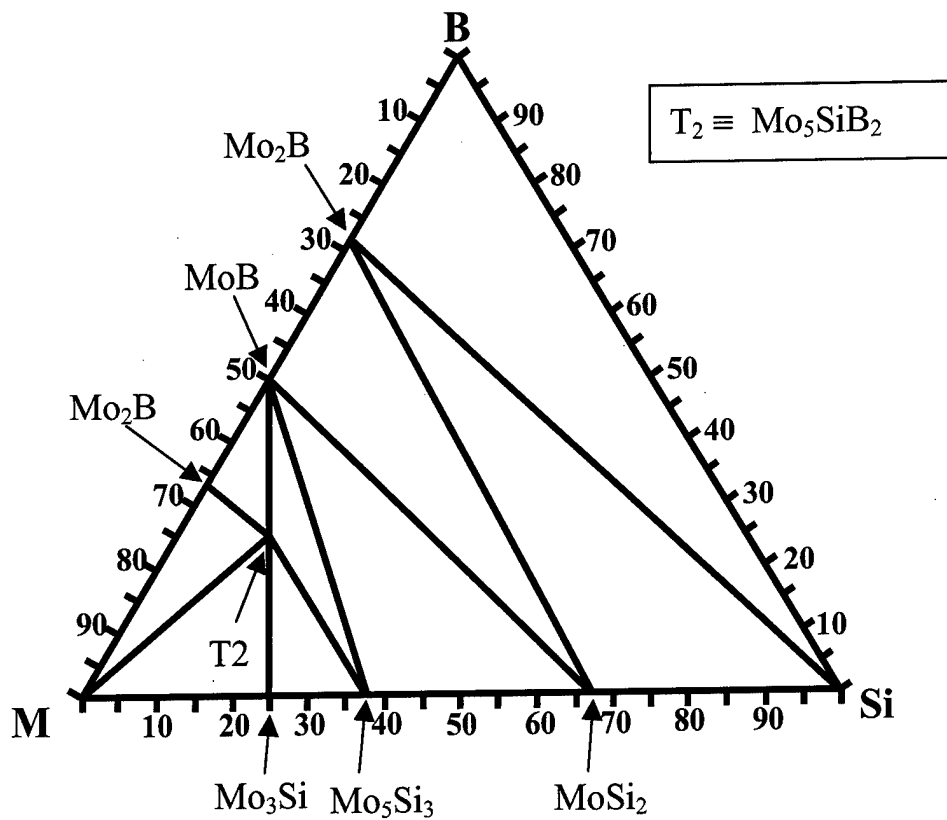


Figure 18 Schematic Isothermal Section of the Mo-Si-B System at 1600°C

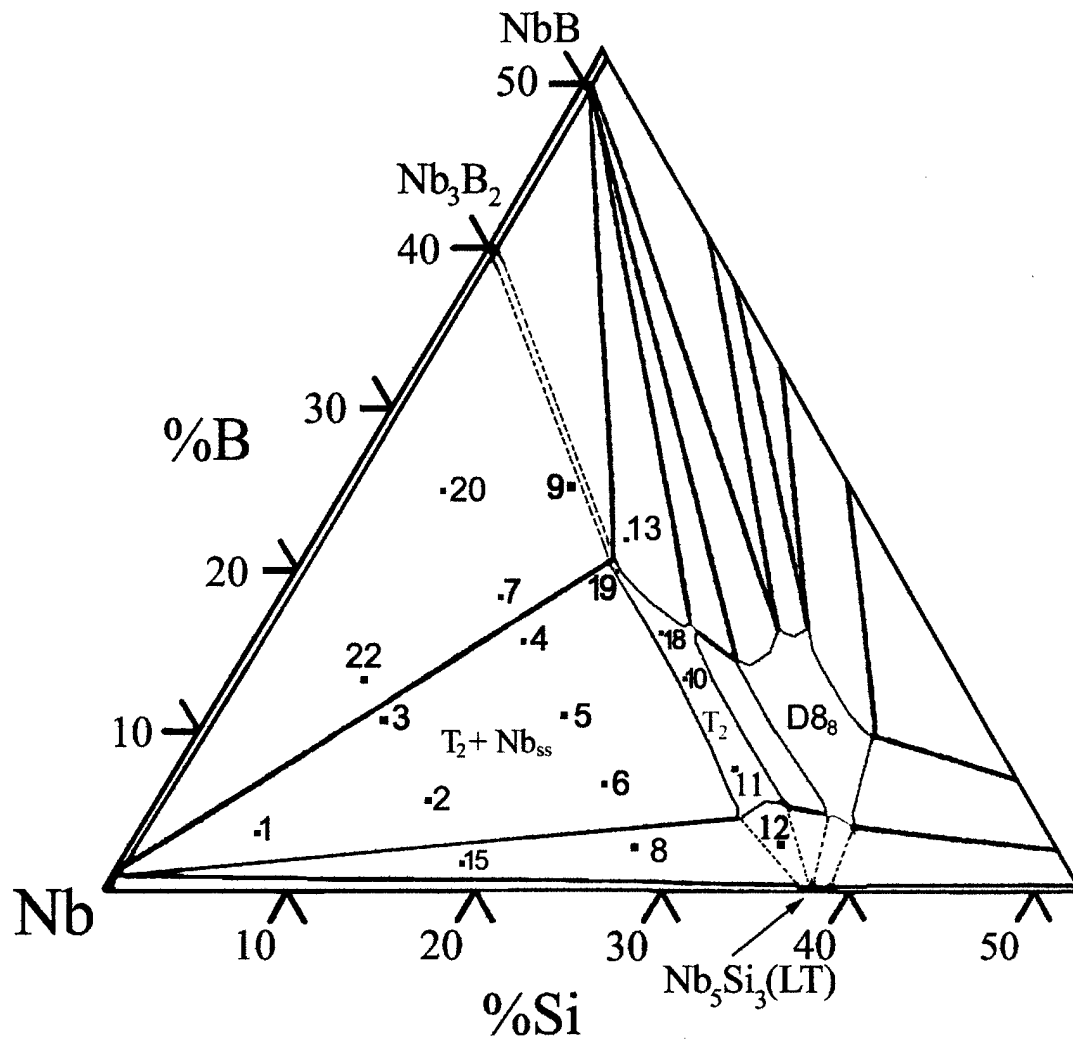


Figure 19 Nb-Si-B Isothermal Section at 1600°C. The numbered points refer to the alloy compositions of this study

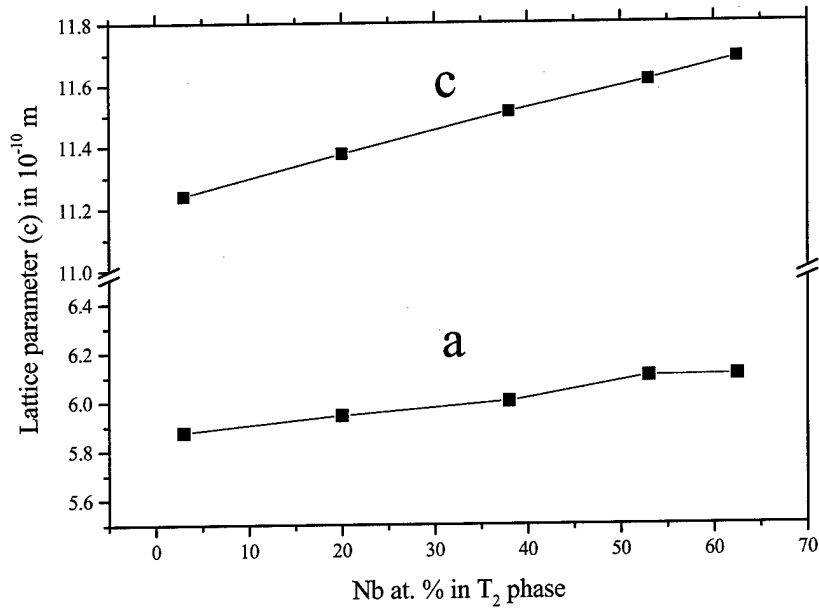


Figure 20 The effect of Nb substitution in the lattice parameters of the T₂ phase

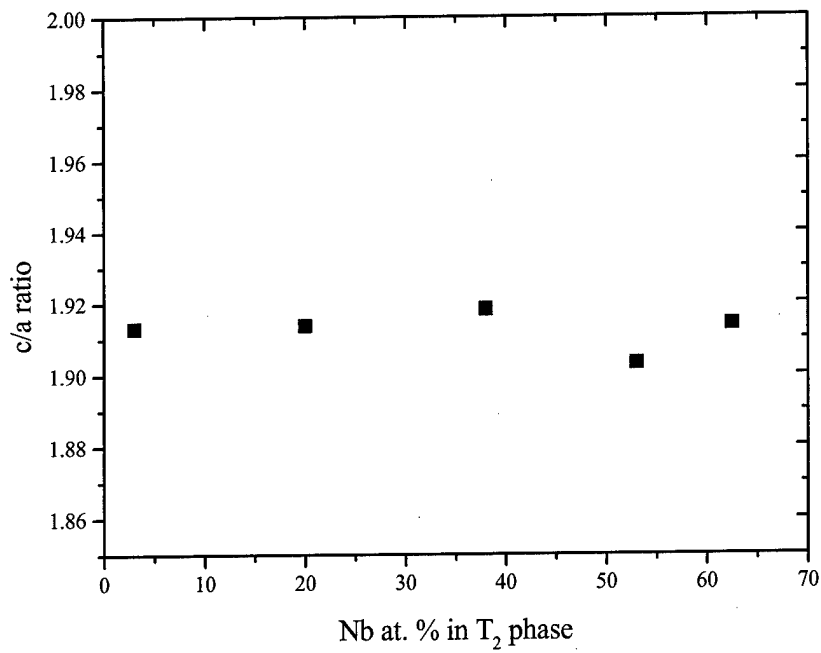


Figure 21 The c/a ratio in Nb-substituted T₂ phase.